International Journal of Mathematical Archive-5(4), 2014, 221-253
Available online through www.ijma.info ISSN 2229 – 5046

MHD MIXED CONVECTION PERIODIC FLOW IN A ROTATING VERTICAL POROUS CHANNEL WITH HEAT RADIATION AND HEAT SOURCE AND CHEMICAL REACTION AND SORET EFFECT

Y. Swapna*[1] and S. V. K. Varma[2]

[1]Research Scholar, Department of Mathematics,
Sri Venkateswara University, Tirupati - 517502, (A.P.), India.

[2]Professor, Department of Mathematics,
Sri Venkateswara University, Tirupati - 517502, (A.P.), India.

(Received on: 14-04-14; Revised & Accepted on: 26-04-14)

ABSTRACT

In this paper, we studied the oscillatory mixed convection flow of an electrically conducting viscous incompressible fluid through a porous medium in a vertical channel. The entire system rotates about an axis perpendicular to the planes of the plates of the channel and a uniform magnetic field is also applied along this axis of rotation. The magnetic Reynolds number is assumed to be small enough so that the induced magnetic field is neglected. The expressions for the velocity field, temperature field and concentration field are obtained analytically. The effects of various emerging physical parameters on the velocity, temperature and concentration are discussed through graphs in detail.

Keywords: *Chemical reaction, Periodic flow, MHD, porous medium, rotating system, heat radiation, Soret effect.*

1. INTRODUCTION

In the past few decades several researchers have been investigated the problems on heat and mass transfer in view of their application to astrophysics, geophysics and engineering. Chemical reaction can be codified either heterogeneous or homogeneous processes. Its effect depends on the nature of the reaction whether the reaction is heterogeneous or homogeneous. A reaction is of order n, if the reaction rate is proportional to the nth power of concentration. In particular, a reaction is of first order, if the rate of reaction is directly proportional to concentration itself. In nature, the presence of pure air or water is not possible. Some foreign mass may be present naturally mixed with air or water. The presence of foreign mass in air or water causes some kind of chemical reaction. The study of such type of chemical reaction processes is useful for improving a number of chemical technologies, such as food processing, polymer production and manufacturing of ceramics or glassware. Chambre and Young (1958) investigated the effect of homogeneous first order chemical reactions in the neighborhood of a flat plate for destructive and generative reactions. The effect of first order reaction on the flow past an impulsively started infinite vertical plate with uniform heat flux and mass transfer was analyzed by Das *et al*. (1994). Anjalidevi and Kandasamy (2000) studied the influence of chemical reaction on the flow in the presence of heat transfer and magnetic field. The effect of chemical reaction on unsteady flow past an impulsively started infinite vertical plate was investigated by Muthukumaraswamy and Ganesan (2001). Raptis and Perdikis (2006) analyzed numerically the steady two-dimensional flow in the presence of chemical reaction over a non-linearly semi-infinite stretching sheet. The effects of thermal radiation, chemical reaction and rotation on unsteady MHD viscoelastic slip flow were investigated by Manglesh and Gorla (2012).

Corresponding author: Y. Swapna*[1]
[1]Research Scholar, Department of Mathematics,
Sri Venkateswara University, Tirupati - 517502, (A.P.), India.
E-mail: swapnaanand100@gmail.com

Moreover the study of the interaction of the Coriolis force with the electromagnetic force is of great importance. In particular, rotating MHD flows in porous media with heat transfer is one of the important current topics due to its applications in thermo fluid transport modeling in magnetic geosystems Armstead (1982), meteorology, MHD power generators, turbo machinery, solidification process in metallurgy, and in some astrophysical problems. It is generally thought that the existence of the geomagnetic field is due to finite amplitude instability of the Earth's core. Since most cosmic bodies are rotators, the study of convective motions in a rotating electrically conducting fluid is essential in understanding better the magnetohydrodynamics of the interiors of the Earth and other planets. It has motivated a number of studies on convective motions in hydromagnetic rotating systems, which can provide explanations for the observed variations in the geomagnetic field. The rotating flow subjected to different physical effects has been studied by many authors (Vidyanidhu and Nigam, 1967; Jana and Datta, 1977; Singh, 2000; Singh and Mathew, 2012; Singh, 2012).

The aim of the present analysis is to study an oscillatory mixed convection flow of an electrically conducting viscous incompressible fluid through a porous medium in a vertical channel. The entire system rotates about an axis perpendicular to the planes of the plates of the channel and a uniform magnetic field is also applied along this axis of rotation. The magnetic Reynolds number is assumed to be small enough so that the induced magnetic field is neglected. The expressions for the velocity field, temperature field and concentration field are obtained analytically. The effects of various emerging physical parameters on the velocity, temperature and concentration are discussed through graphs in detail.

2. MATHEMATICAL ANALYSIS

Consider the flow of a viscous, incompressible and electrically conducting fluid in a rotating vertical porous channel.

In order to derive basic equations for the problem under consideration following assumptions are made:
I. The flow considered is unsteady and laminar.
II .The fluid is finitely conducting and with constant physical properties.
III .A magnetic field of uniform strength is applied normal to the flow.
IV .The magnetic Reynolds number is taken to be small enough so that the induced magnetic field is neglected.
V. Hall effect, polarization and electrical effects are neglected.
VI. It is assumed that the fluid is optically thin with relatively low density.
VII. The entire system rotates about an axis perpendicular to the plates.
VIII. Since the plates are infinite so all physical quantities except pressure depend only on z^* and t^* .

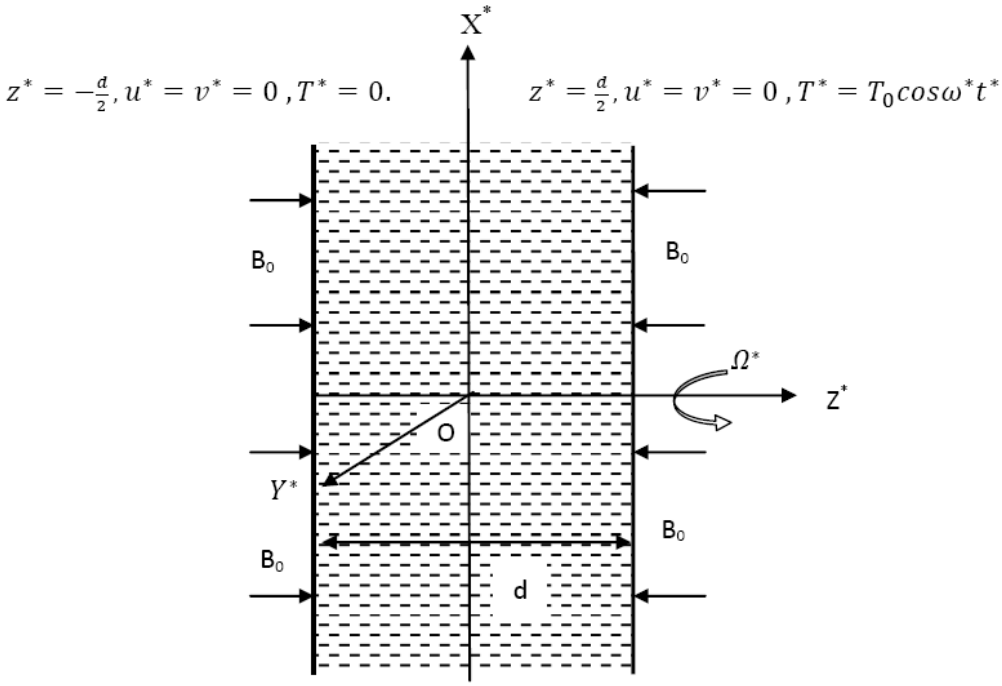

Fig.1. Physical configuration of the physical problem.

An unsteady flow of a viscous incompressible and electrically conducting fluid through porous medium in a vertical channel is considered. The two infinite plates of the vertical channel distance'd' apart. A coordinate system is chosen such that the X^*-axis is oriented upward along the centerline of the channel and Z^*-axis taken perpendicular to the

planes of the plates lying in $Z^* = \pm\frac{d}{2}$ .The non-uniform temperature of the plate at $Z^* = \pm\frac{d}{2}$ is assumed to be varying periodically with time. The Z^*-axis is considered to be the axis of rotation about which the fluid and the plates are assumed to be rotating as a solid body with a constant angular velocity Ω^*. A transverse magnetic field of uniform strength $B(0,0,B_0)$ is also applied along the axis of rotation. The velocity may reasonably be assumed with its components along X^*, Y^*, Z^* directions as $V(u^*, v^*, 0)$.The equation of continuity is then satisfied identically. Using the velocity and the magnetic field distribution as stated above the magneto hydrodynamic (MHD) flow in the rotating channel is governed by the following Cartesian equations:

$$\frac{\partial u^*}{\partial t^*} = -\frac{1}{\rho}\frac{\partial p^*}{\partial x^*} + \upsilon\frac{\partial^2 u^*}{\partial z^{*2}} + 2\Omega^* v^* - \frac{\sigma B_0^2 u^*}{\rho} + g\beta T^* + g\beta_c C^* - \frac{\upsilon}{k^*}u^* \tag{1}$$

$$\frac{\partial v^*}{\partial t^*} = -\frac{1}{\rho}\frac{\partial p^*}{\partial y^*} + \upsilon\frac{\partial^2 v^*}{\partial z^{*2}} - 2\Omega^* u^* - \frac{\sigma B_0^2 v^*}{\rho} - \frac{\upsilon}{k^*}v^* \tag{2}$$

$$0 = -\frac{1}{\rho}\frac{\partial p^*}{\partial z^*} \tag{3}$$

$$\rho c_p \frac{\partial T^*}{\partial t^*} = k\frac{\partial^2 T^*}{\partial z^{*2}} - 4\alpha^2 T^* + \frac{Q^*}{\rho c_p}T^* \tag{4}$$

$$\frac{\partial C^*}{\partial t^*} = D\frac{\partial^2 C^*}{\partial z^{*2}} + D_1\frac{\partial^2 T^*}{\partial z^{*2}} - k_1^* C^* \tag{5}$$

where ρ is the density, υ is the kinematic viscosity, p* is the modified pressure, t* is the time, σ is the electric conductivity, g is the acceleration due to gravity, k is the thermal conductivity, c_p is the specific heat at constant pressure and α is the mean radiation absorption coefficient. Equation (3) shows the constancy of the hydrodynamic pressure along the axis of rotation. We shall assume now that the fluid flows under the influence of pressure gradient varying periodically with time in the X*-axis is of the form

$$-\frac{1}{\rho}\frac{\partial p^*}{\partial y^*} = A\cos\omega^* t^* \tag{6}$$

Where A is a constant.

The boundary conditions relevant to the problem are:

$$z^* = \frac{d}{2} : u^* = v^* = 0, T^* = T_0\cos\omega^* t^*, C^* = C_0\cos\omega^* t^* \tag{7}$$

$$z^* = -\frac{d}{2} : u^* = v^* = 0, T^* = 0, C^* = 0 \tag{8}$$

where T_0 is the mean temperature, C_0 is the mean concentration and ω^* is the frequency of oscillation.

On introducing the following Non-dimensional parameters in to equations

$$\eta = \frac{z^*}{d}, x = \frac{x^*}{d}, y = \frac{y^*}{d}, u = \frac{u^*}{U}, v = \frac{v^*}{U}, T = \frac{T^*}{T_0}, C = \frac{C^*}{C_0}, t = \frac{t^* U}{d}, \omega = \frac{\omega^* d}{U}, p = \frac{p^*}{\rho U^2} \tag{9}$$

where U is the mean axial velocity,'*' represents the dimensional physical quantities,

In equations (1) to (5), we get the following non-dimensional governing equations:

$$\mathrm{Re}\frac{\partial u}{\partial t} = -\mathrm{Re}\frac{\partial p}{\partial x} + \frac{\partial^2 u}{\partial \eta^2} + 2\Omega v - M^2 u + GrT + GmC - \frac{u}{k} \tag{10}$$

$$\mathrm{Re}\frac{\partial v}{\partial t} = -\mathrm{Re}\frac{\partial p}{\partial y} + \frac{\partial^2 v}{\partial \eta^2} - 2\Omega u - M^2 v - \frac{v}{k} \tag{11}$$

$$P\mathrm{e}\frac{\partial T}{\partial t} = \frac{\partial^2 T}{\partial \eta^2} - N^2 T + SPeT \tag{12}$$

$$\mathrm{Re}\,Sc\frac{\partial C}{\partial t} = \frac{\partial^2 C}{\partial \eta^2} + S_0 Sc\frac{\partial^2 T}{\partial \eta^2} - k_1 ScC \tag{13}$$

The non-dimensional boundary conditions are:

$$\eta = \frac{1}{2} : u = v = 0, T = \cos\omega t, C = \cos\omega t \tag{14}$$

$$\eta = -\frac{1}{2} : u = v = 0, T = 0, C = 0. \tag{15}$$

For the oscillatory internal flow we shall assume that the fluid flows only under the influence of a non- dimension pressure gradient oscillating in the direction of x-axis only which is of the form

$$-\frac{\partial p}{\partial x} = A\cos\omega t \tag{16}$$

3. SOLUTION OF THE PROBLEM

Now combine equations (10) and (11) into single equation by introducing a complex function of the form $F = u + iv,$, we get

$$\mathrm{Re}\frac{\partial F}{\partial t} = \mathrm{Re}\,A\cos\omega t + \frac{\partial^2 F}{\partial \eta^2} - (M^2 + 2i\Omega + k^{-1})F + GrT + GmC \tag{17}$$

With corresponding boundary conditions as

$$\eta = \frac{1}{2} : F = 0, T = \cos\omega t, C = \cos\omega t. \tag{18}$$

$$\eta = -\frac{1}{2} : F = 0, T = 0, C = 0. \tag{19}$$

In order to solve equations (17) and (12),(13) under the boundary conditions (18) and (19), we assume in complex notations the solution of the problem as

$$F(\eta, t) = F_0(\eta)e^{i\omega t}, T = \theta_0(\eta)e^{i\omega t}, C = \phi_0(\eta)e^{i\omega t}, -\frac{\partial y}{\partial x} = Ae^{i\omega t} \tag{20}$$

The boundary conditions (18) and (19) in complex notations can also be written as

$$\eta = \frac{1}{2} : F = 0, T = e^{i\omega t}, C = e^{i\omega t} \tag{21}$$

$$\eta = -\frac{1}{2} : F = 0, T = 0, C = 0 \tag{22}$$

Substituting these expressions in equations (12) & (13) and (17), we get

$$\frac{d^2 F_0}{d\eta^2} - m^2 F_0 = -\mathrm{Re}\,A - Gr\theta_0 - Gm\phi_0 \tag{23}$$

$$\frac{d^2 \theta_0}{d\eta^2} - n^2 \theta_0 = 0 \tag{24}$$

$$\frac{d^2\phi_0}{d\eta^2} - p^2\phi_0 = -r\frac{\sinh\left(n\left(\eta+\frac{1}{2}\right)\right)}{\sinh(n)} \tag{25}$$

where $m=\sqrt{M^2+2i\Omega+k^{-1}+i\omega\,\mathrm{Re}}, n=\sqrt{N^2+i\omega Pe-SPe},\ p=\sqrt{i\omega\,\mathrm{Re}\,Sc+k_1Sc}$ and $r=S_0Scn^2, q=\dfrac{r}{n^2-p^2}$.

The Transformed boundary conditions reduce to

$$\eta=\frac{1}{2}: F_0=0, \theta_0=1, \phi_0=1 \tag{26}$$

$$\eta=-\frac{1}{2}: F_0=0, \theta_0=0, \phi_0=0 \tag{27}$$

The Ordinary differential equations (23), (24) and (25) are solved under the boundary conditions (26) and (27) for the velocity, the temperature, the concentration profiles. The solution of the problem is obtained as

$$\begin{aligned} u(\eta,t) = {} & [\frac{\mathrm{Re}\,A}{m^2}(1-\frac{\cosh(m\eta)}{\cosh(m/2)}) + \frac{Gr}{n^2-m^2}[\frac{\sinh(m(\eta+1/2))}{\sinh(m)} - \frac{\sinh(n(\eta+1/2))}{\sinh(n)}] \\ & + \frac{Gm}{p^2-m^2}\{\frac{\sinh(m(\eta+1/2))}{\sinh(m)} - \frac{\sinh(p(\eta+1/2))}{\sinh(p)}\} + \frac{Gmq}{n^2-m^2}(\frac{\sinh(m(\eta+1/2))}{\sinh(m)} - \frac{\sinh(n(\eta+1/2))}{\sinh(n)}) \\ & - \frac{Gmq}{p^2-m^2}\{\frac{\sinh(m(\eta+1/2))}{\sinh(m)} - \frac{\sinh(p(\eta+1/2))}{\sinh(p)}\}]e^{i\omega t} \end{aligned} \tag{28}$$

(29)

$$T(\eta,t) = [\frac{\sinh(n(\eta+1/2))}{\sinh(n)}]e^{i\omega t} \tag{30}$$

$$C(\eta,t) = \{\frac{\sinh(p(\eta+1/2))}{\sinh(p)} - q(\frac{\sinh(p(\eta+1/2))}{\sinh(p)} - \frac{\sinh(n(\eta+1/2))}{\sinh(n)})\}e^{i\omega t} \tag{31}$$

From the velocity field we can now obtain the skin-friction τ_L at the left plate in terms of its amplitude and phase angle as

$$\tau_L = \left(\frac{\partial u}{\partial \eta}\right)_{\eta=-\frac{1}{2}} = |F|\cos(\omega t+\varphi), \tag{32}$$

$$\begin{aligned} F_r + iF_i = {} & \frac{\mathrm{Re}\,A}{m}\tanh\frac{m}{2} + \frac{Gr}{n^2-m^2}\left\{\frac{m}{\sinh m} - \frac{n}{\sinh n}\right\} \\ & + \frac{Gm}{p^2-m^2}\left\{\frac{m}{\sinh m} - \frac{p}{\sinh p}\right\} + \frac{Gmq}{n^2-m^2}\left\{\frac{m}{\sinh m} - \frac{n}{\sinh n}\right\} \\ & - \frac{Gmq}{p^2-m^2}\left\{\frac{m}{\sinh m} - \frac{p}{\sinh p}\right\} \end{aligned} \tag{33}$$

The amplitude is $|F| = \sqrt{F_r^2+F_i^2}$ and the phase angle $\varphi = \tan^{-1}\dfrac{F_i}{F_r}$ (34)

From the temperature field given in equation (30) the heat transfer coefficient Nu (Nusslet number) in terms of its amplitude and phase angle can be obtained as

$$Nu = \left(\frac{\partial T}{\partial \eta}\right)_{\eta=-\frac{1}{2}} = |H|\cos(\omega t+\psi) \tag{35}$$

where $H_r + iH_i = \dfrac{n}{\sinh n}$ (36)

The amplitude $|H|$ and the phase angle ψ of the heat transfer coefficient Nu are given by

$$|H| = \sqrt{H_r^2 + H_i^2} \text{ and } \psi = \tan^{-1}\frac{H_i}{H_r} \tag{37}$$

From the concentration field given in equation (31) the mass transfer coefficient Sh (Sherwood number) in terms of its amplitude and phase angle can be obtained as

$$Sh = \left(\frac{\partial C}{\partial \eta}\right)_{\eta=-\frac{1}{2}} = |G|\cos(\omega t + \theta) \tag{38}$$

where $G_r + iG_i = \dfrac{p}{\sinh p} - q\left\{\dfrac{p}{\sinh p} - \dfrac{n}{\sinh n}\right\}$ (39)

The amplitude $|H|$ and the phase angle ψ of the heat transfer coefficient Nu are given by

$$|G| = \sqrt{G_r^2 + G_i^2} \text{ and } \theta = \tan^{-1}\frac{G_i}{G_r} \tag{40}$$

4. RESULTS AND DISCUSSIONS

(a) Velocity Profiles

In order to study the effects of various physical parameters $\mathrm{Re}, A, N, M, Gr, Gm, k, k1, \omega, \Omega, Pe, S, So$ and Sc on velocity we plotted Figs. 2 to 15. From Fig. 2, it is found that the velocity u decreases with increasing rotation parameter Ω. The velocity profiles initially remain parabolic with maximum at the centre of the channel for small values of rotation parameter Ω and then as rotation parameter increases the velocity profiles flatten. For large value of rotation parameter Ω (= 20) the maximum of velocity profiles no longer occurs at the centre of the channel but shift towards the walls of the channel. That is for large rotation there occur boundary layers near the walls of the channel. From Fig. 3, it is observed that the velocity u increases with an increase in Reynolds number Re. Fig. 4 shows that, the velocity u increases with increasing pressure gradient A. From Fig. 5, it is seen that, the velocity u goes on decreasing with increasing Hartmann number M. From Fig. 6, it is noted that the velocity decreases with an increase in radiation parameter N. From Fig. 7, it is observed that, the velocity decrease with increasing Peclet number Pe. From Fig. 8, it is found that the velocity increases with an increase in Grashof number Gr. Further, it is found that the maximum of the velocity profiles shifts toward right half of the channel due to the greater buoyancy force in this part of the channel due to the presence of hotter plate. From Fig. 9, it is seen that the velocity increases with increasing Gm. From Fig. 10, it is noticed that velocity decreases with increasing frequency of oscillation ω. From Fig. 11, it is found that the velocity increases with increasing Darcy number k. From Fig. 12, it is observed that velocity decreases with increasing $k1$. From Fig. 13, it is found that the velocity increases with an increase in S. From Fig. 14, it is noted that velocity decreases with increasing So. From Fig. 15, it is observed that velocity decreases with increasing Sc.

In order to study the effects of various physical parameters $\mathrm{Re}, A, N, M, Gr, Gm, k, k1, \Omega, Pe, S, So$ and Sc on amplitude of the skin friction $|F|$ we have plotted Figs. 16 to 28. From Fig. 16, it is observed that the amplitude of the skin friction $|F|$ decreases with increasing frequency of oscillation ω. Further it is observed that, the amplitude of the skin friction $|F|$ decreases with increasing Ω. From Fig. 17, it is found that the amplitude of the skin friction $|F|$ increases with an increase in Re. From Fig. 18, it is noticed that the amplitude of the skin friction $|F|$ increases with increasing pressure gradient A. From Fig. 19, it is seen that amplitude of the skin friction $|F|$ decreases with an increase in M. From Fig. 20, it is found that amplitude of the skin friction $|F|$ first decreases and then increases with increasing N. From Fig. 21, it is noted that the amplitude of the skin friction $|F|$ first increases and then decreases with increasing Peclet number Pe. From Fig. 22, it is observed that the amplitude of the skin friction $|F|$ first increases and then decreases with increasing Grashof number Gr. From Fig. 23, it is noticed that the

amplitude of the skin friction $|F|$ first increases and then decreases with increasing Gm. From Fig. 24, it is found that the amplitude of the skin friction $|F|$ increases with increasing Darcy number k. From Fig. 25, it is seen that the amplitude of the skin friction $|F|$ decreases with increasing k_1. From Fig. 26, it is observed that the amplitude of the skin friction $|F|$ increases with an increase in S. From Fig. 27, it is noted that the amplitude of the skin friction $|F|$ decreases with increasing So. From Fig. 28, it is found that the amplitude of the skin friction $|F|$ decreases with increasing Sc.

In order to study the effects of various physical parameters $\mathrm{Re}, A, N, M, Gr, Gm, k, k1, \Omega, Pe, S, So$ and Sc on the phase angle of the skin friction φ we have plotted Figs. 29 to 41. From Fig. 29, it is observed that the phase angle of the skin friction φ decreases with increasing Ω. From Fig. 30, it is found that the phase angle of the skin friction φ initially increases and then decreases with an increase in Re. From Fig. 31, it is noticed that the phase angle of the skin friction φ first increases and then decreases with increasing pressure gradient A. From Fig. 32, it is seen that the phase angle of the skin friction φ increases with an increase in M. From Fig. 33, it is found that the phase angle of the skin friction φ first increases and then decreases with increasing N. From Fig. 34, it is noted that the phase angle of the skin friction φ first decreases and then increases with increasing Peclet number Pe. From Fig. 35, it is observed that the phase angle of the skin friction φ decreases with increasing Grashof number Gr. From Fig. 36, it is noticed that the phase angle of the skin friction φ first decreases and then increases with increasing Gm. From Fig. 37, it is found that the phase angle of the skin friction φ decreases with increasing Darcy number k. From Fig. 38, it is seen that the phase angle of the skin friction φ first increases and then decreases with increasing k_1. From Fig. 39, it is observed that the phase angle of the skin friction φ first decreases and then increases with an increase in S. From Fig. 40, it is noted that the phase angle of the skin friction φ first decreases and then increases with increasing So. From Fig. 41, it is found that the phase angle of the skin friction φ first decreases and then increases with increasing Sc.

(b) Temperature Profiles

In order to see the effects of various physical parameters $\omega, Pe, S,$ and N on the temperature T we have plotted Figs. 42 to 45. From Fig. 42, it is found that the temperature T decreases with increasing ω. From Fig. 43, it is observed that the temperature T decreases with increasing N. From Fig. 44, it is noted that the temperature T decreases with an increase in Pe. From Fig. 45, it is seen that the temperature T increases with increasing S.

In order to see the effects of various physical parameters $Pe, S,$ and N on the amplitude of the Nusselt number $|H|$ we have plotted Figs. 46 to 48. From Fig. 46, it is observed that the amplitude of the Nusselt number $|H|$ decreases with increasing N. From Fig. 47, it is noted that the amplitude of the Nusselt number $|H|$ first increases and then decreases with an increase in Pe. From Fig. 48, it is seen that the amplitude of the Nusselt number $|H|$ increases with increasing S.

In order to see the effects of various physical parameters $Pe, S,$ and N on the phase angle of the Nusselt number ψ we have plotted Figs. 49 to 51. It is found that there is a phase lag initially for small values of the frequency of oscillation ω and thereafter the phase oscillates between phase lag and the phase lead. From Fig. 49, it is observed that the phase angle of the Nusselt number ψ increases with increasing N. From Fig. 50, it is noticed that the phase angle of the Nusselt number ψ oscillates with increasing Peclet number Pe. From Fig. 51, it is found that the phase angle of the Nusselt number ψ also oscillates with increasing S.

(c) Concentration Profiles

In order to study the effects of various physical parameters $\mathrm{Re}, N, k1, \omega, Pe, S, So$ and Sc on concentration C we plotted Figs. 52 to 59. From Fig. 52, it is observed that the concentration C increases with an increase in Reynolds

number Re. From Fig. 53, it is noted that the concentration C first increases and then decreases with an increase in radiation parameter N. From Fig. 54, it is noticed that concentration C decreases with increasing frequency of oscillation ω. From Fig. 55, it is observed that, the concentration C first increases and then decreases with increasing Peclet number Pe. From Fig. 56, it is found that the concentration C increases with an increase in k_1. From Fig. 57, it is found that the concentration C first decreases and then increases with an increase in S. From Fig. 58, it is noted that concentration C decreases with increasing So. From Fig. 59, it is observed that concentration C decreases with increasing Sc.

In order to study the effects of various physical parameters $\mathrm{Re}, N, k1, Pe, S, So$ and Sc on the amplitude $|G|$ we plotted Figs. 60 to 66. From Fig. 60, it is observed that the amplitude $|G|$ initially increases and then decrease with an increase in Reynolds number Re. From Fig. 61, it is noted that the amplitude $|G|$ first increases and then decreases with an increase in radiation parameter N. From Fig. 62, it is observed that, the amplitude $|G|$ first increases and then decreases with increasing Peclet number Pe. From Fig. 63, it is found that the amplitude $|G|$ decreases with an increase in k_1. From Fig. 64, it is found that the amplitude $|G|$ increases with an increase in S. From Fig. 65, it is noted that amplitude $|G|$ increases with increasing So. From Fig. 59, it is observed that amplitude $|G|$ first decreases and then increases with increasing Sc.

In order to study the effects of various physical parameters $\mathrm{Re}, N, k1, Pe, S, So$ and Sc on the phase angle θ we plotted Figs. 67 to 73. It is found that the phase angle θ oscillates with $\omega, \mathrm{Re}, N, k1, Pe, S, So$ and Sc.

REFERENCES

1. Anjalidevi, S. P. and Kandasamy, R. Effects of chemical reaction heat and mass transfer on MHD flow past a semi-infinite plate, Z. Angew. Mathematics and Mechanics, 80(2000), 697-701.
2. Armstead, H. C. Geothermal Energy, EN Spon(1982). London.
3. Chambre, P. L. and Young, J. D. On the diffusion of a chemically reactive species in a laminar boundary layer flow, Physics of Fluids, 1(1958), 48-54.
4. Das, U.N., Deka, R.K. and Soundalgekar, V. M. Effects of mass transfer on flow past an impulsively started infinite vertical plate with constant heat flux and chemical reaction, Forsch. Ingenieurwes, 60(1994), 284- 287.
5. Jana, R.N. and Datta, N, Couette flow and heat transfer in a rotating system, Acta Mech., 26(1977), 301-306.
6. Manglesh, A. and Gorls, M.G. The effects of thermal radiation, chemical reaction and rotation on unsteady MHD viscoelastic slip flow, Global Journal of Science Frontier Research Mathematics and Decision Sciences, 12 (14) (2012), 1-15.
7. Muthucumaraswamy, R. and Ganesan, P. First order chemical reaction on flow past an impulsivelystarted vertical plate with uniform heat and mass flux, Acta Mechanica, 147(2001), 45-57.
   Raptis, A, and Perdikis, C. Viscous flow over a non-linearly stretching sheet in the presence of a chemical reaction and magnetic field, International Journal of Non-Linear Mechanics, 41(2006), 527-529.
8. Singh, K.D. An oscillatory hydromagnetic Couette flow in a rotating system, J. Appl. Math. and Mech., 80(2000), 429-432.
9. Singh, K.D. and Mathew, A, An oscillatory free convective flow through porous medium in a rotating vertical porous channel, Global J of Science Frontier Research, 12 (3) (2012), 51-64.
10. Singh, K.D. Exact solution of MHD mixed convection periodic flow in a rotating vertical channel with heat radiation, International Journal of Physical and Mathematical Sciences, 3(1) (2012), 14-30.
11. Vidyanidhu, V. and Nigam, S.D. Secondary flow in a rotating channel, J. Math. and Phys. Sci., 1(1967), 85-100.

© 2014, IJMA. All Rights Reserved

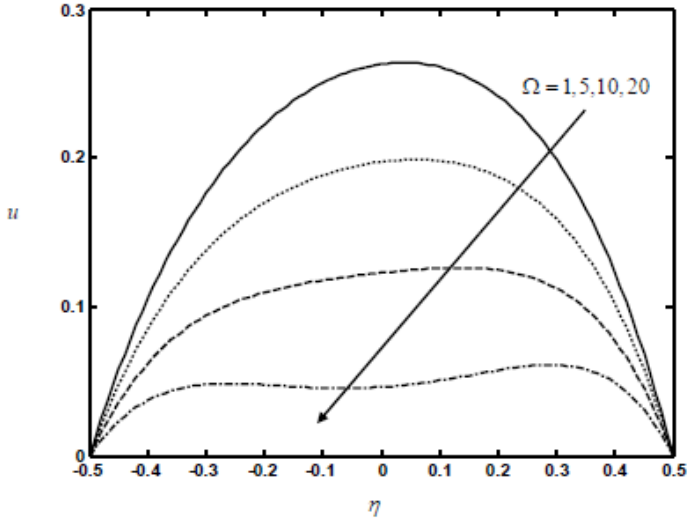

Fig. – 2: Velocity profiles for different Ω with $\mathrm{Re}=1$, $A=5$, $t=0$, $N=1$, $M=2$, $Pe=0.7$, $\omega=5$, $Gr=1$, $Gm=1$, $k=0.1$, $k1=0.5$, $S=0.1$, $S_0=2.5$ and $Sc=0.22$.

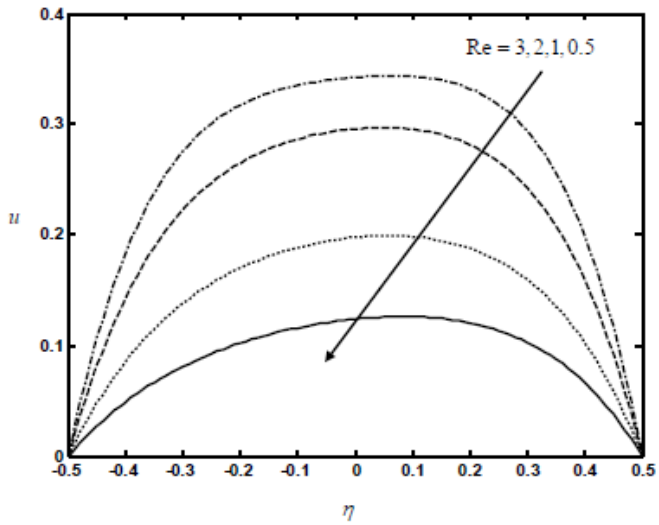

Fig. – 3: Velocity profiles for different Re with $\Omega=5$, $A=5$, $t=0$, $N=1$, $M=2$, $Pe=0.7$, $\omega=5$, $Gr=1$, $Gm=1$, $k=0.1$, $k1=0.5$, $S=0.1$, $S_0=2.5$ and $Sc=0.22$.

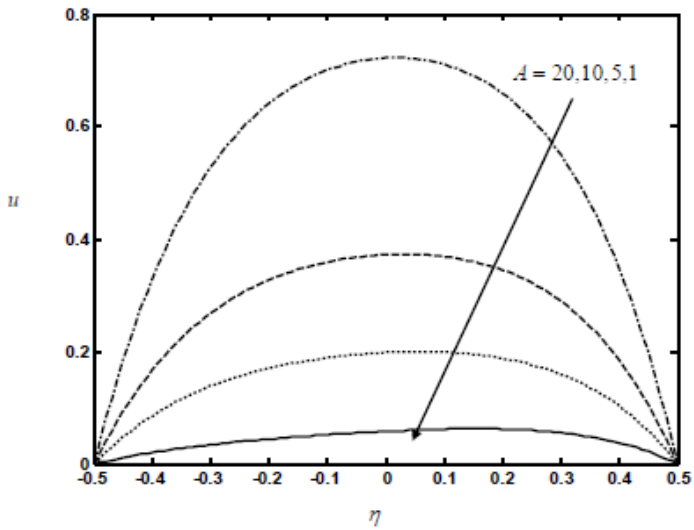

Fig. – 4: Velocity profiles for different A with $\mathrm{Re}=1$, $\Omega=5$, $t=0$, $N=1$, $M=2$, $Pe=0.7$, $\omega=5$, $Gr=1$, $Gm=1$, $k=0.1$, $k1=0.5$, $S=0.1$, $S_0=2.5$ and $Sc=0.22$.

© 2014, IJMA. All Rights Reserved

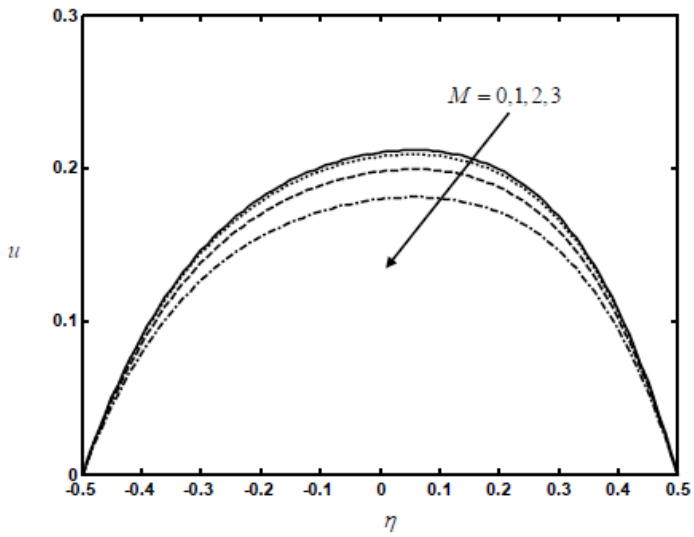

Fig. – 5: Velocity profiles for different M with $\mathrm{Re} = 1$, $A = 5$, $t = 0$, $N = 1$, $\Omega = 5$, $Pe = 0.7$, $\omega = 5$, $Gr = 1$, $Gm = 1$, $k = 0.1$, $k1 = 0.5$, $S = 0.1$, $S_0 = 2.5$ and $Sc = 0.22$.

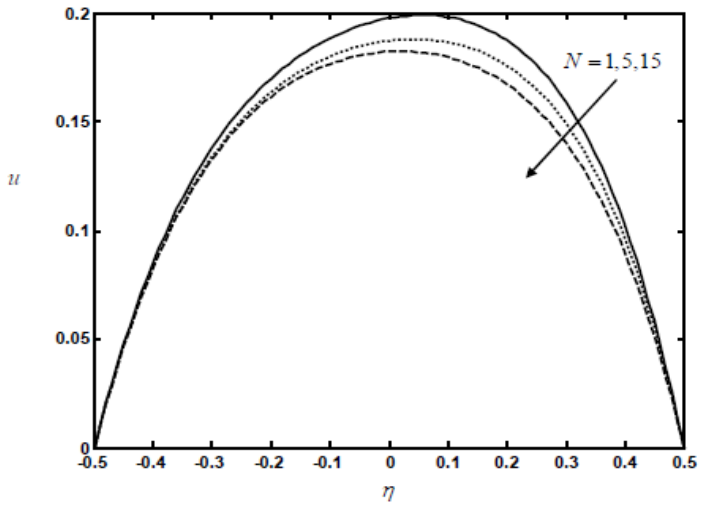

Fig. – 6: Velocity profiles for different N with $\mathrm{Re} = 1$, $A = 5$, $t = 0$, $\Omega = 5$, $M = 2$, $Pe = 0.7$, $\omega = 5$, $Gr = 1$, $Gm = 1$, $k = 0.1$, $k1 = 0.5$, $S = 0.1$, $S_0 = 2.5$ and $Sc = 0.22$.

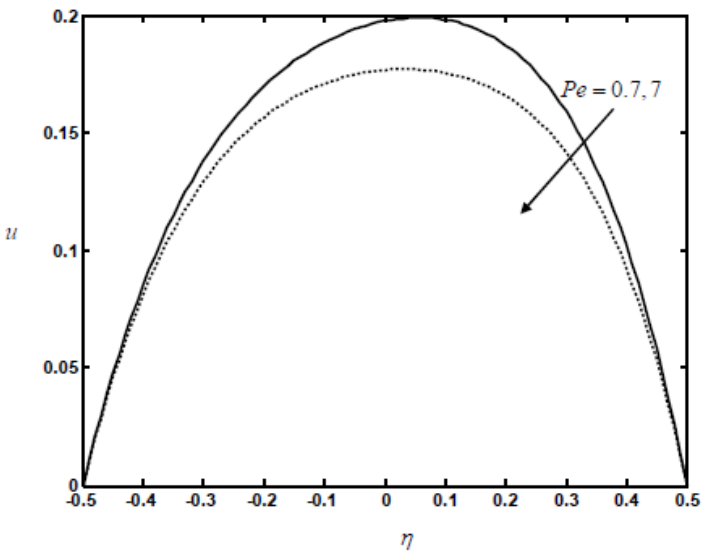

Fig. – 7: Velocity profiles for different Pe with $\mathrm{Re} = 1$, $A = 5$, $t = 0$, $N = 1$, $M = 2$, $\Omega = 5$, $\omega = 5$, $Gr = 1$, $Gm = 1$, $k = 0.1$, $k1 = 0.5$, $S = 0.1$, $S_0 = 2.5$ and $Sc = 0.22$.

© 2014, IJMA. All Rights Reserved

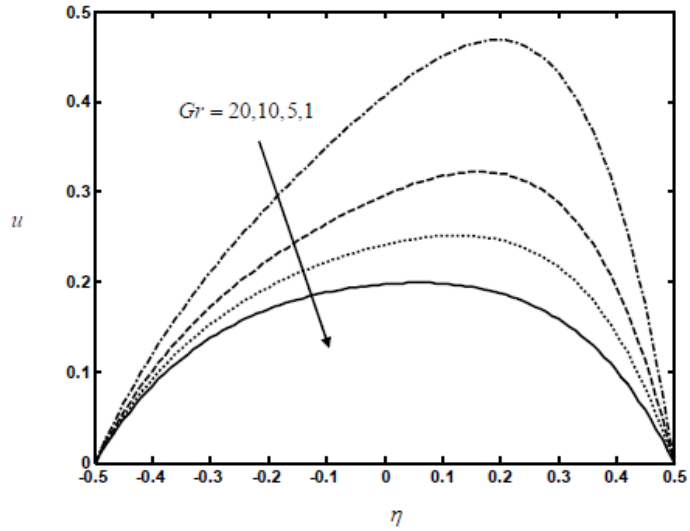

Fig. – 8: Velocity profiles for different Gr with $\mathrm{Re}=1$, $A=5$, $t=0$, $N=1$, $M=2$, $Pe=0.7$, $\omega=5$, $\Omega=5$, $Gm=1$, $k=0.1$, $k1=0.5$, $S=0.1$, $S_0=2.5$ and $Sc=0.22$.

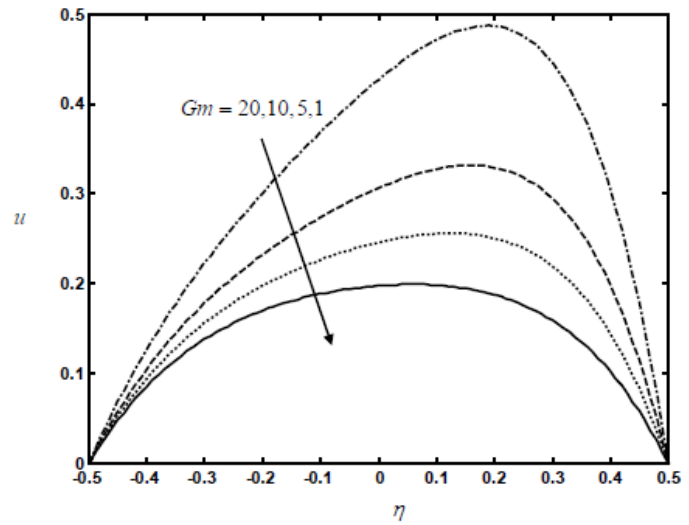

Fig. – 9: Velocity profiles for different Gm with $\mathrm{Re}=1$, $A=5$, $t=0$, $N=1$, $M=2$, $Pe=0.7$, $\omega=5$, $Gr=1$, $\Omega=5$, $k=0.1$, $k1=0.5$, $S=0.1$, $S_0=2.5$ and $Sc=0.22$.

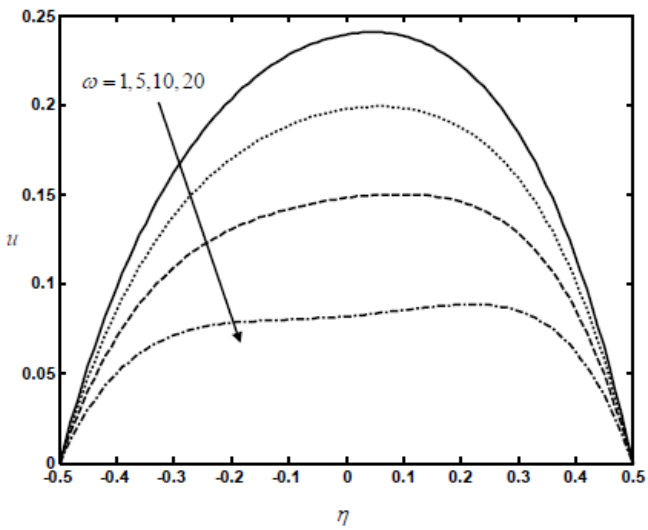

Fig. – 10: Velocity profiles for different ω with $\mathrm{Re}=1$, $A=5$, $t=0$, $N=1$, $M=2$, $Pe=0.7$, $Gm=1$, $Gr=1$, $\Omega=5$, $k=0.1$, $k1=0.5$, $S=0.1$, $S_0=2.5$ and $Sc=0.22$.

© 2014, IJMA. All Rights Reserved

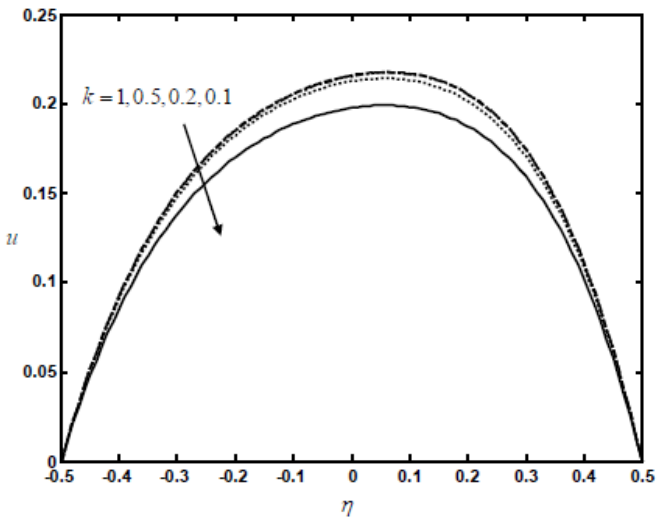

Fig. – 11: Velocity profiles for different k with $\mathrm{Re}=1$, $A=5$, $t=0$, $N=1$, $M=2$, $Pe=0.7$, $\omega=5$, $Gr=1$, $Gm=1$, $\Omega=5$, $k1=0.5$, $S=0.1$, $S_0=2.5$ and $Sc=0.22$.

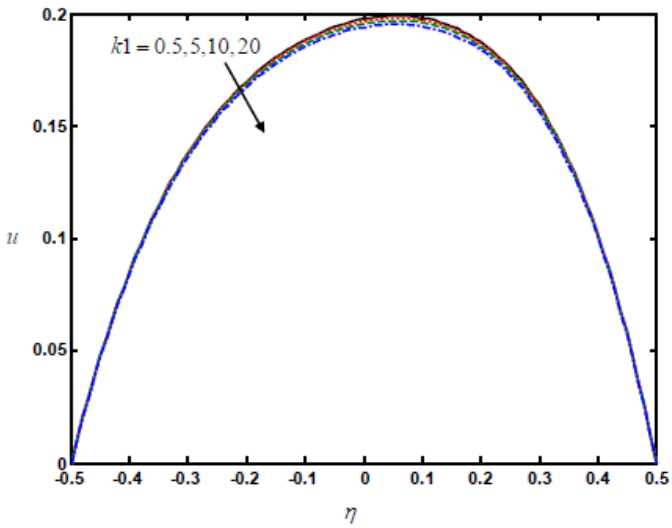

Fig. – 12: Velocity profiles for different $k1$ with $\mathrm{Re}=1$, $A=5$, $t=0$, $N=1$, $M=2$, $Pe=0.7$, $\omega=5$, $Gr=1$, $Gm=1$, $\Omega=5$, $k=0.1$, $S=0.1$, $S_0=2.5$ and $Sc=0.22$.

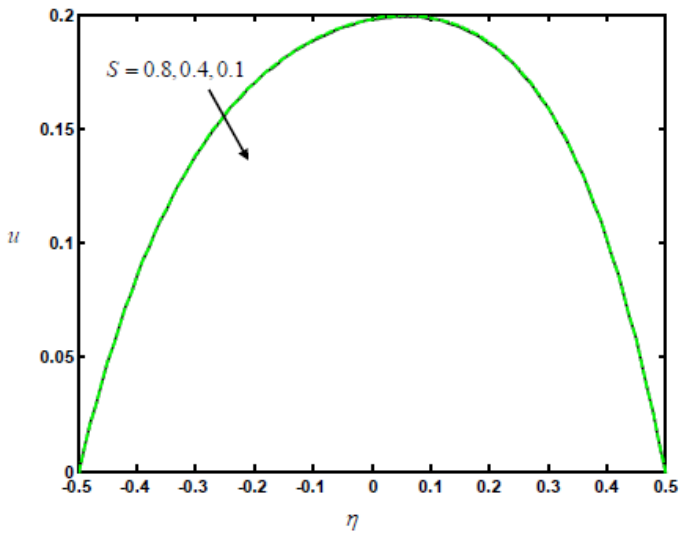

Fig. - 13: Velocity profiles for different S with $\mathrm{Re}=1$, $A=5$, $t=0$, $N=1$, $M=2$, $Pe=0.7$, $\omega=5$, $Gm=1$, $Gr=1$, $\Omega=5$, $k=0.1$, $K1=0.5$, $S_0=2.5$ and $Sc=0.22$.

© 2014, IJMA. All Rights Reserved

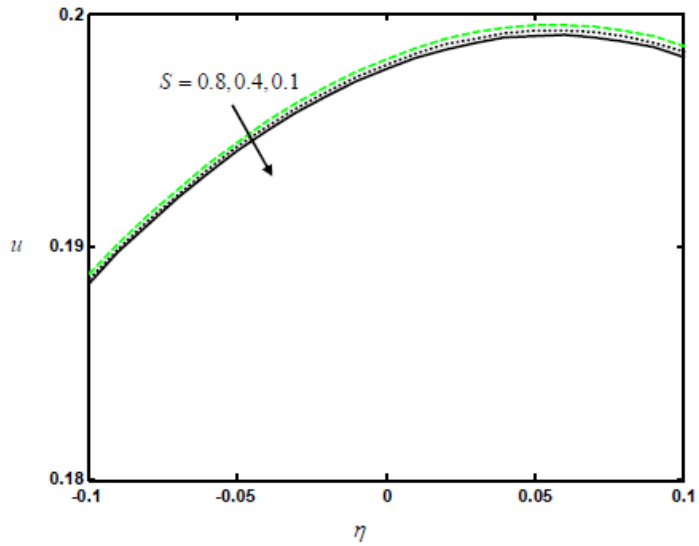

Fig. – 13:(a) Enlargement of Fig. 12.

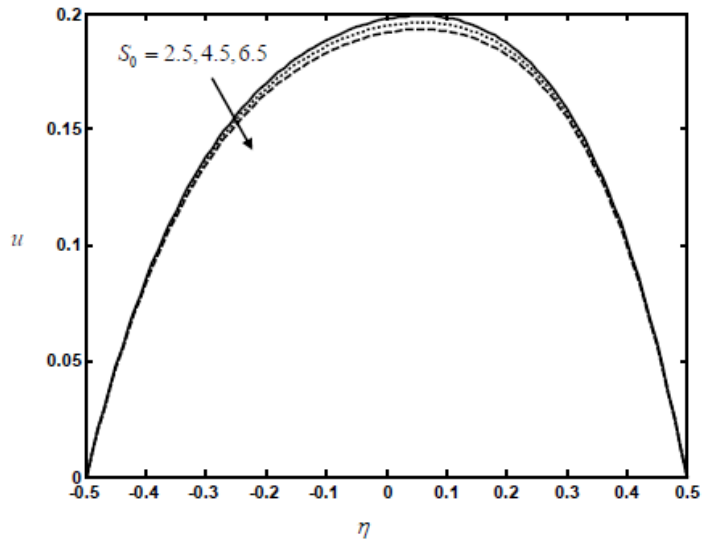

Fig. – 14: Velocity profiles for different S_o with $\mathrm{Re} = 1$, $A = 5$, $t = 0$, $N = 1$, $M = 2$, $Pe = 0.7$, $\omega = 5$, $Gm = 1$, $Gr = 1$, $\Omega = 5$, $k = 0.1$, $K_1 = 0.5$, $S = 0.1$, and $Sc = 0.22$.

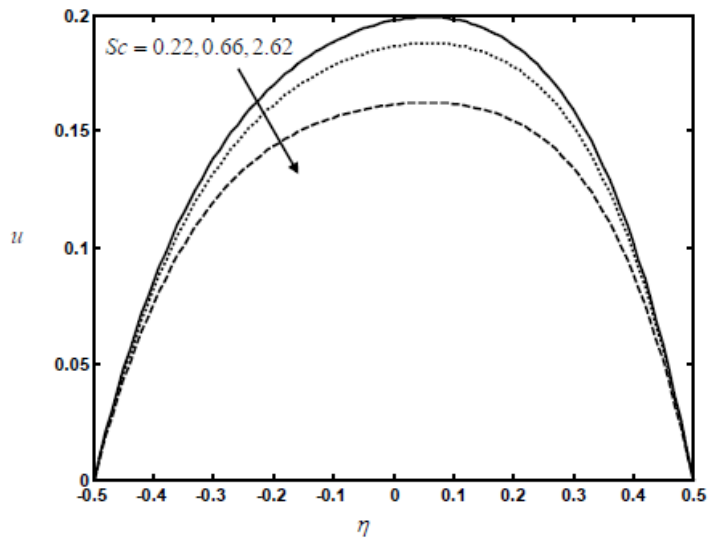

Fig. – 15: Velocity profiles for different Sc with $\mathrm{Re} = 1$, $A = 5$, $t = 0$, $N = 1$, $M = 2$, $Pe = 0.7$, $\omega = 5$, $Gm = 1$, $Gr = 1$, $\Omega = 5$, $k = 0.1$, $k_1 = 0.5$, $S_0 = 2.5$ and $S = 0.1$,.

© 2014, IJMA. All Rights Reserved

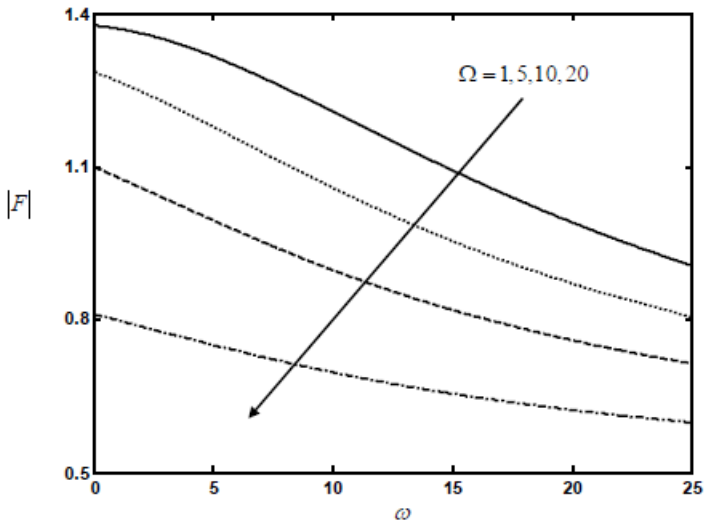

Fig. – 16: Amplitude of the skin-friction for different Ω with $\mathrm{Re}=1$, $A=5$, $t=0$, $N=1$, $M=2$, $Pe=0.7$, $Gr=1, Gm=1$, $k=0.1$, $k1=0.5$, $S=0.1$, $S_0=2.5$ and $Sc=0.22$.

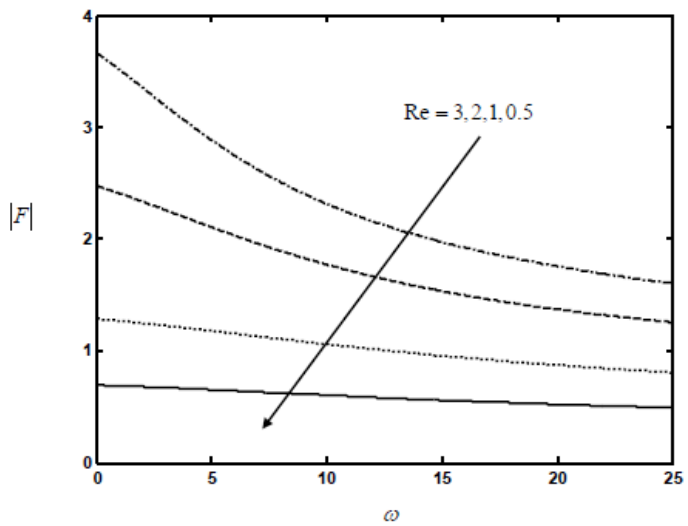

Fig. – 17: Amplitude of the skin-friction for different Re with $\Omega = 5$, $A=5$, $t=0$, $N=1$, $M=2$, $Pe=0.7$, $Gr=1, Gm=1$, $k=0.1$, $k1=0.5$, $S=0.1$, $S_0=2.5$ and $Sc=0.22$.

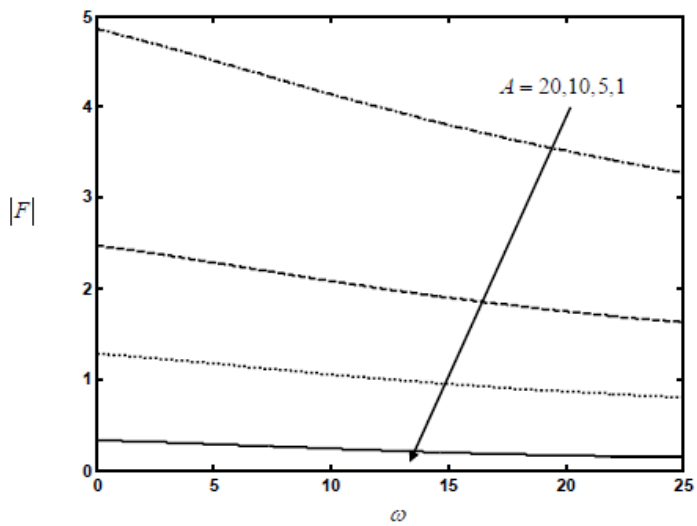

Fig. – 18: Amplitude of the skin-friction for different A with $\mathrm{Re}=1$, $\Omega = 5$, $t=0$, $N=1$, $M=2$, $Pe=0.7$, $Gr=1, Gm=1$, $k=0.1$, $k1=0.5$, $S=0.1$, $S_0=2.5$ and $Sc=0.22$.

© 2014, IJMA. All Rights Reserved

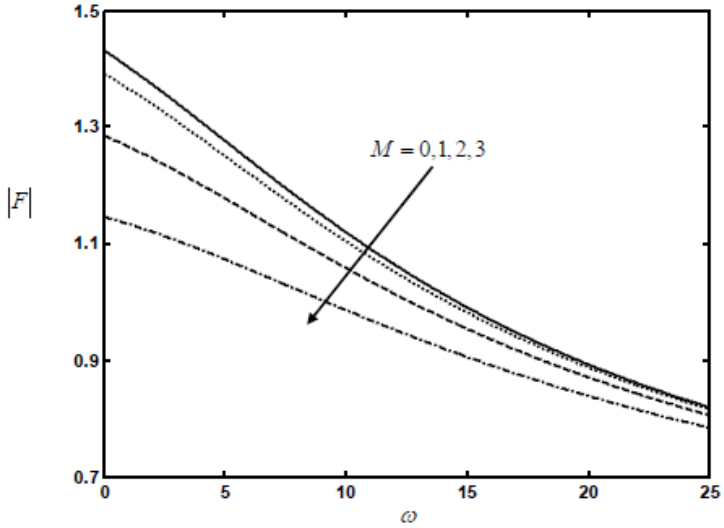

Fig. – 19: Amplitude of the skin-friction for different M with $\mathrm{Re} = 1$, $A = 5$, $t = 0$, $N = 1$, $\Omega = 5$, $Pe = 0.7$, $Gr = 1, Gm = 1$, $k = 0.1$, $k1 = 0.5$, $S = 0.1$, $S_0 = 2.5$ and $Sc = 0.22$.

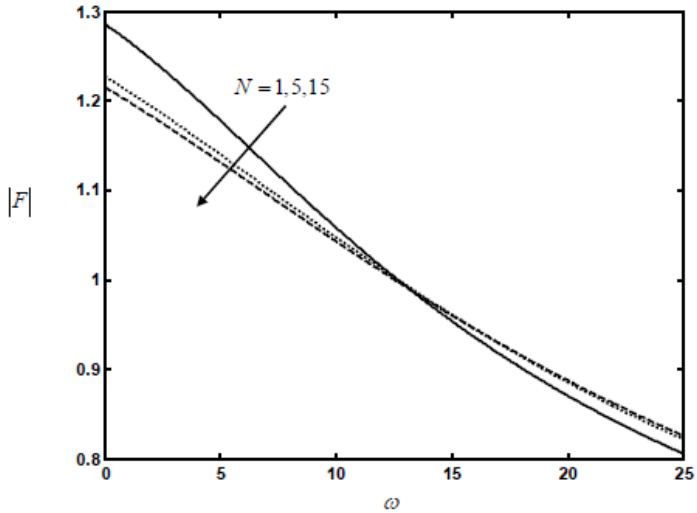

Fig. – 20: Amplitude of the skin-friction for different N with $\mathrm{Re} = 1$, $A = 5$, $t = 0$, $\Omega = 5$, $M = 2$, $Pe = 0.7$, $\omega = 5, Gr = 1, Gm = 1$, $k = 0.1$, $k1 = 0.5$, $S = 0.1$, $S_0 = 2.5$ and $Sc = 0.22$

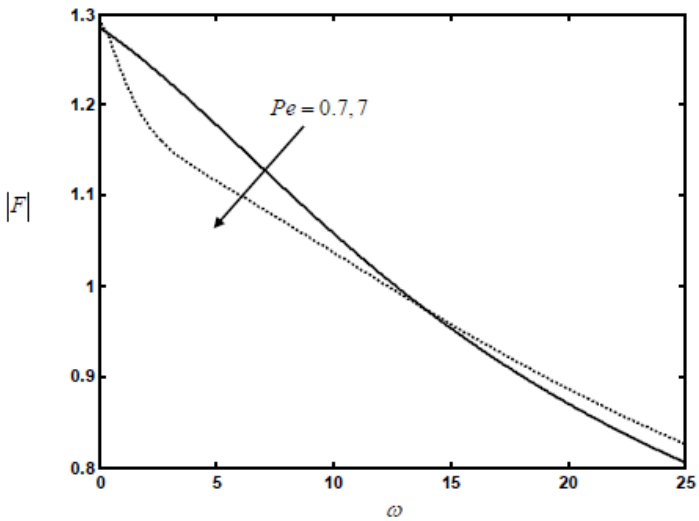

Fig. – 21: Amplitude of the skin-friction for different Pe with $\mathrm{Re} = 1$, $A = 5$, $t = 0$, $N = 1$, $M = 2$, $\Omega = 5$, $Gr = 1, Gm = 1$, $k = 0.1$, $k1 = 0.5$, $S = 0.1$, $S_0 = 2.5$ and $Sc = 0.22$.

© 2014, IJMA. All Rights Reserved

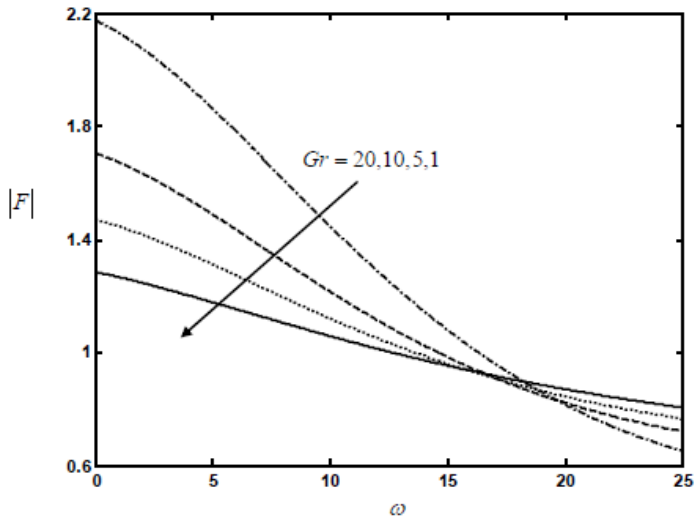

Fig. – 22: Amplitude of the skin-friction for different Gr with $\mathrm{Re}=1$, $A=5$, $t=0$, $N=1$, $M=2$, $Pe=0.7$, $\Omega=5$, $Gm=1$, $k=0.1$, $k1=0.5$, $S=0.1$, $S_0=2.5$ and $Sc=0.22$.

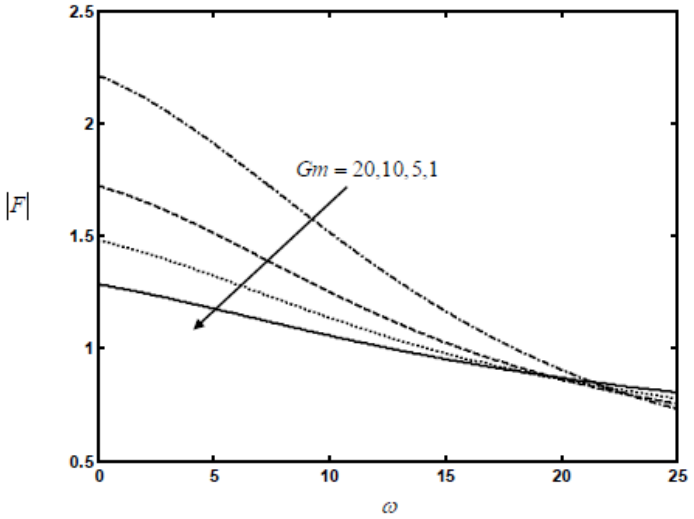

Fig. – 23: Amplitude of the skin-friction for different Gm with $\mathrm{Re}=1$, $A=5$, $t=0$, $N=1$, $M=2$, $Pe=0.7$, $Gr=1$, $\Omega=5$, $k=0.1$, $k1=0.5$, $S=0.1$, $S_0=2.5$ and $Sc=0.22$.

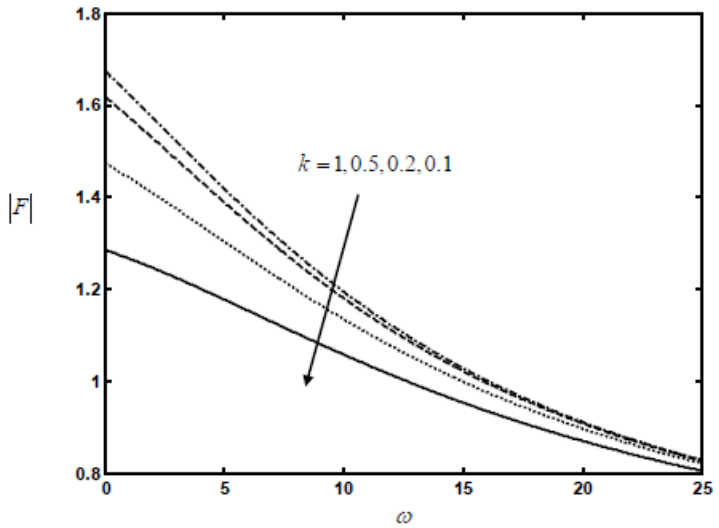

Fig. – 24: Amplitude of the skin-friction for different k with $\mathrm{Re}=1$, $A=5$, $t=0$, $N=1$, $M=2$, $Pe=0.7$, $\omega=5$, $Gr=1$, $Gm=1$, $\Omega=5$, $k1=0.5$, $S=0.1$, $S_0=2.5$ and $Sc=0.22$.

© 2014, IJMA. All Rights Reserved

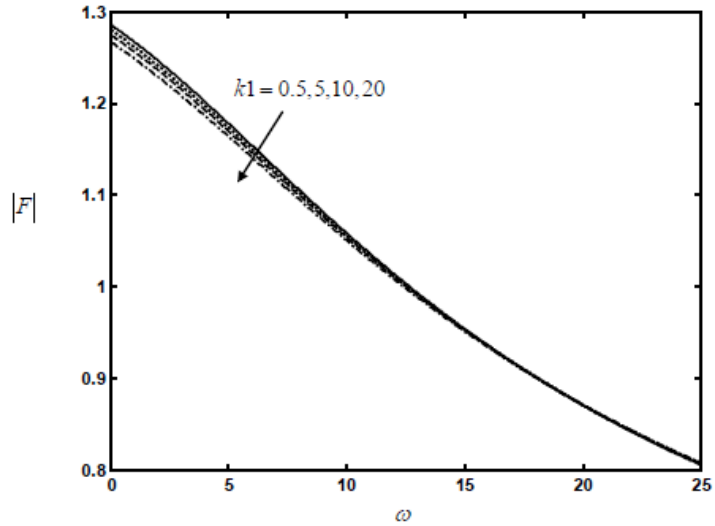

Fig. – 25: Amplitude of the skin-friction for different $k1$ with $\mathrm{Re} = 1$, $A = 5$, $t = 0$, $N = 1$, $M = 2$, $Pe = 0.7$, $Gr = 1, Gm = 1$, $k = 0.1$, $\Omega = 5$, $S = 0.1$, $S_0 = 2.5$ and $Sc = 0.22$.

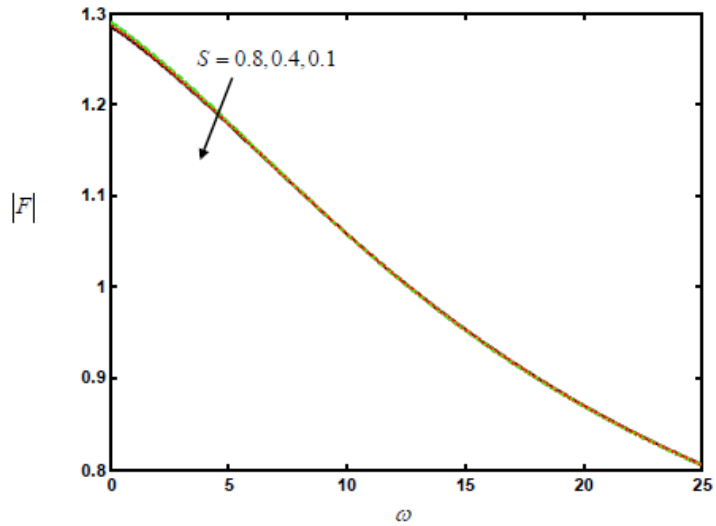

Fig. – 26: Amplitude of the skin-friction for different S with $\mathrm{Re} = 1$, $A = 5$, $t = 0$, $N = 1$, $M = 2$, $Pe = 0.7$, $Gr = 1, Gm = 1$, $k = 0.1$, $k1 = 0.5$, $\Omega = 5$, $S_0 = 2.5$ and $Sc = 0.22$.

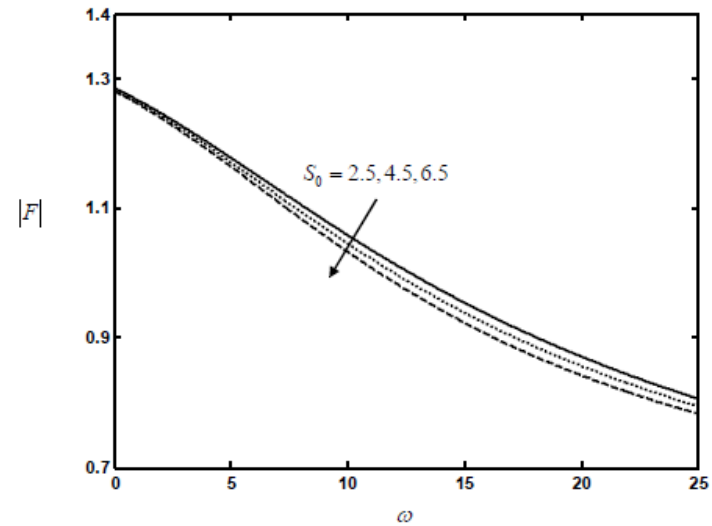

Fig. – 27: Amplitude of the skin-friction for different S_0 with $\mathrm{Re} = 1$, $A = 5$, $t = 0$, $N = 1$, $M = 2$, $Pe = 0.7$, $Gr = 1, Gm = 1$, $k = 0.1$, $k1 = 0.5$, $S = 0.1$, $\Omega = 5$ and $Sc = 0.22$.

© 2014, IJMA. All Rights Reserved

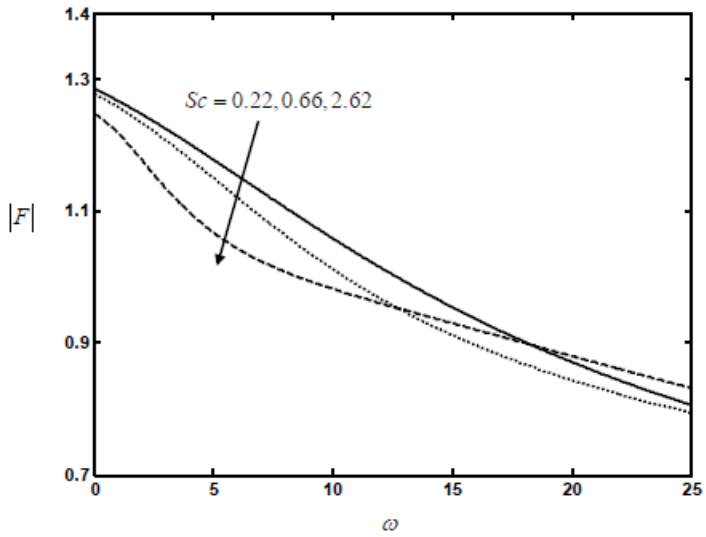

Fig. – 28: Amplitude of the skin-friction for different Sc with $\mathrm{Re} = 1$, $A = 5$, $t = 0$, $N = 1$, $M = 2$, $Pe = 0.7$, $Gr = 1, Gm = 1$, $k = 0.1$, $k1 = 0.5$, $\Omega = 5$, $S = 0.1$ and $S_0 = 2.5$

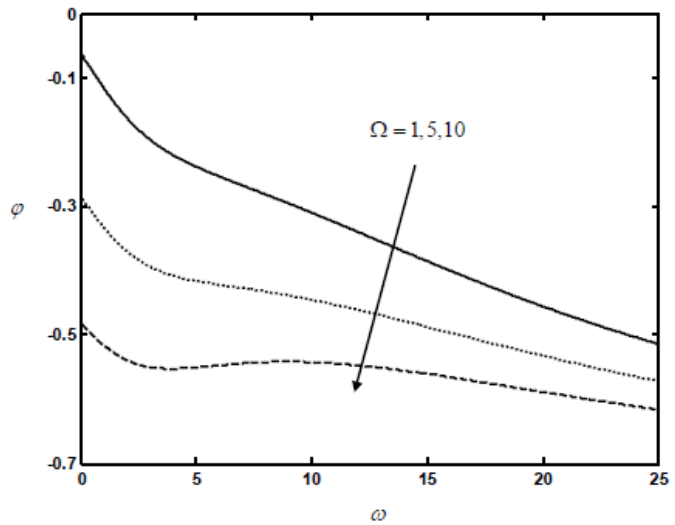

Fig. – 29: Phase angle of the skin-friction for different Ω with $\mathrm{Re} = 1$, $A = 5$, $t = 0$, $N = 1$, $M = 2$, $Pe = 0.7$, $Gr = 1, Gm = 1$, $k = 0.1$, $k1 = 0.5$, $S = 0.1$, $S_0 = 2.5$ and $Sc = 0.22$.

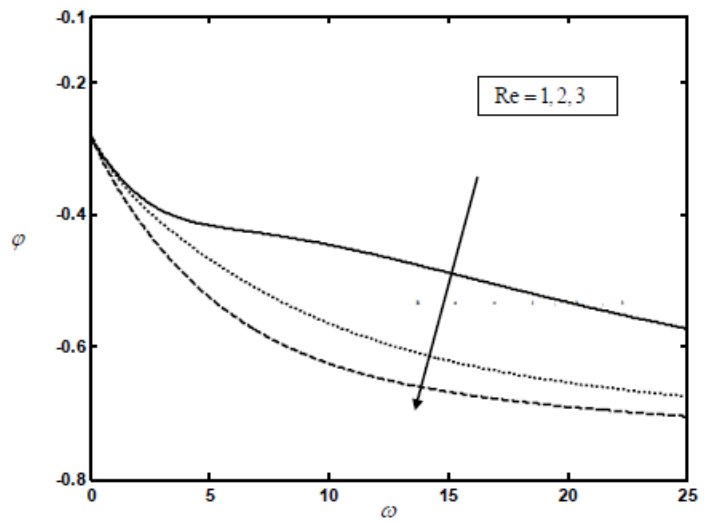

Fig. – 30: Phase angle of the skin-friction for different Re with Ω=5, $A = 5$, $t = 0$, $N = 1$, $M = 2$, $Pe = 0.7$, $Gr = 1, Gm = 1$, $k = 0.1$, $k1 = 0.5$, $S = 0.1$, $S_0 = 2.5$ and $Sc = 0.22$.

© 2014, IJMA. All Rights Reserved

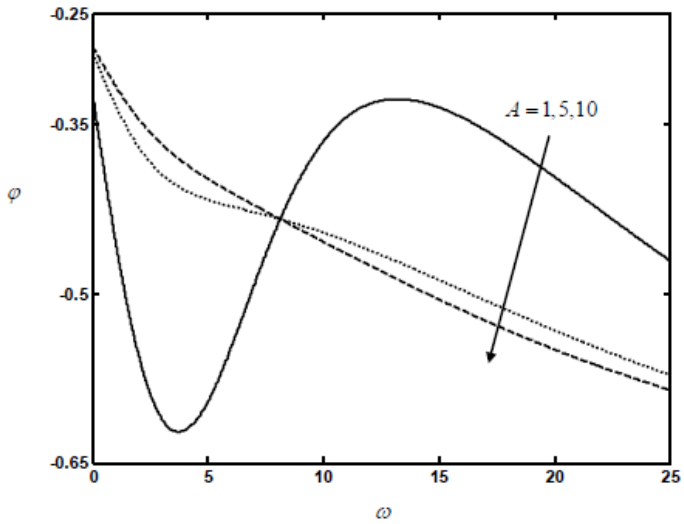

Fig. – 31: Phase angle of the skin-friction for different A with $\mathrm{Re} = 1$, $\Omega = 5$, $t = 0$, $N = 1$, $M = 2$, $Pe = 0.7$, $Gr = 1, Gm = 1$, $k = 0.1$, $k1 = 0.5$, $S = 0.1$, $S_0 = 2.5$ and $Sc = 0.22$.

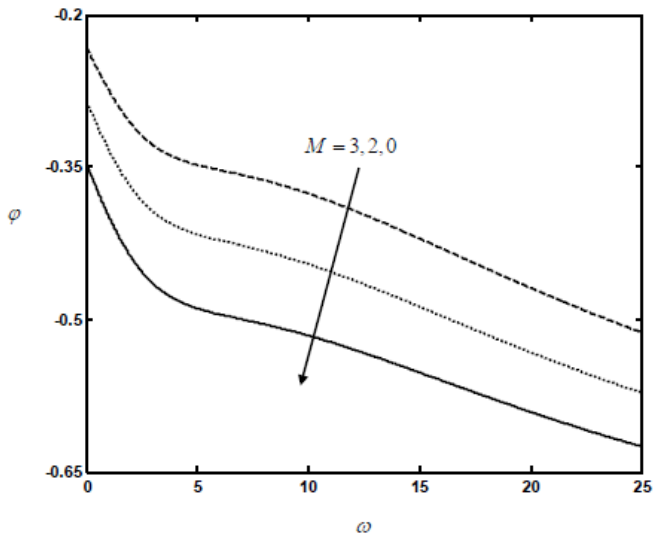

Fig. – 32: Phase angle of the skin-friction for different M with $\mathrm{Re} = 1$, $A = 5$, $t = 0$, $N = 1$, $\Omega = 5$, $Pe = 0.7$, $Gr = 1, Gm = 1$, $k = 0.1$, $k1 = 0.5$, $S = 0.1$, $S_0 = 2.5$ and $Sc = 0.22$.

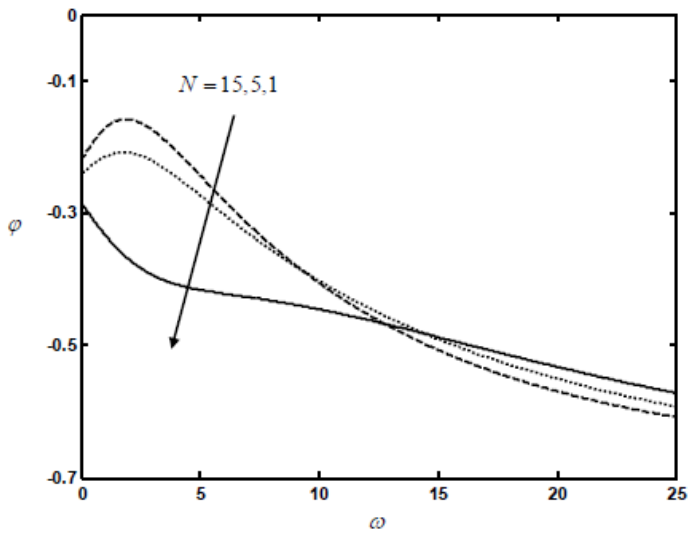

Fig. – 33: Phase angle of the skin-friction for different N with $\mathrm{Re} = 1$, $A = 5$, $t = 0$, $\Omega = 5$, $M = 2$, $Pe = 0.7$, $Gr = 1, Gm = 1$, $k = 0.1$, $k1 = 0.5$, $S = 0.1$, $S_0 = 2.5$ and $Sc = 0.22$.

© 2014, IJMA. All Rights Reserved

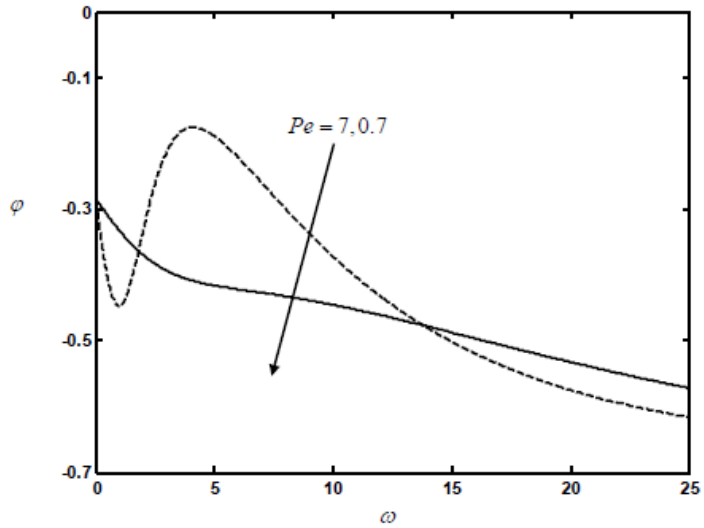

Fig. – 34: Phase angle of the skin-friction for different *Pe* with $\mathrm{Re}=1$, $A=5$, $t=0$, $N=1$, $M=2$, $\Omega=5$, $Gr=1, Gm=1$, $k=0.1$, $k1=0.5$, $S=0.1$, $S_0=2.5$ and $Sc=0.22$.

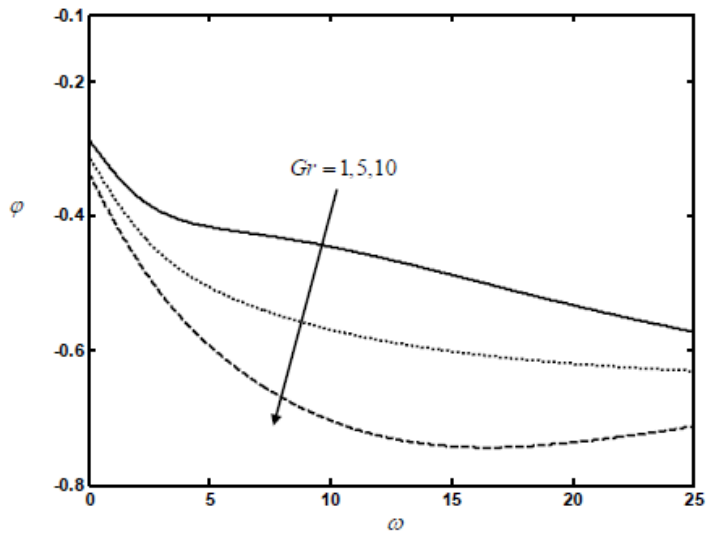

Fig. – 35: Phase angle of the skin-friction for different *Gr* with $\mathrm{Re}=1$, $A=5$, $t=0$, $N=1$, $M=2$, $Pe=0.7$, $\Omega=5$, $Gm=1$, $k=0.1$, $k1=0.5$, $S=0.1$, $S_0=2.5$ and $Sc=0.22$.

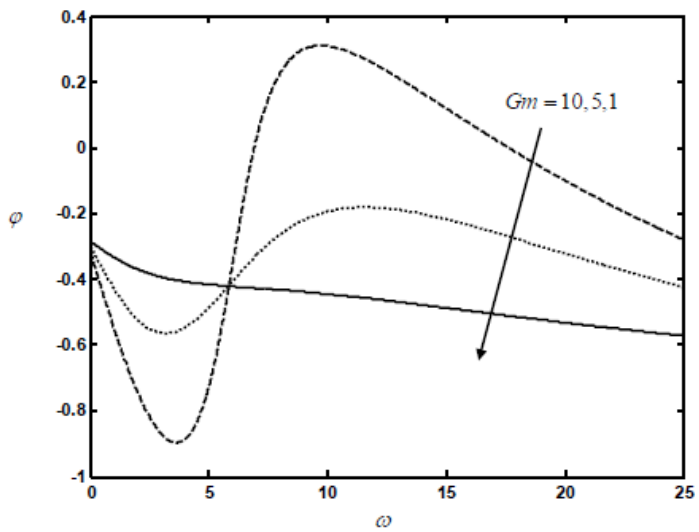

Fig. 36 Phase angle of the skin-friction for different *Gm* with $\mathrm{Re}=1$, $A=5$, $t=0$, $N=1$, $M=2$, $Pe=0.7$, $Gr=1$, $\Omega=5$, $k=0.1$, $k1=0.5$, $S=0.1$, $S_0=2.5$ and $Sc=0.22$.

© 2014, IJMA. All Rights Reserved

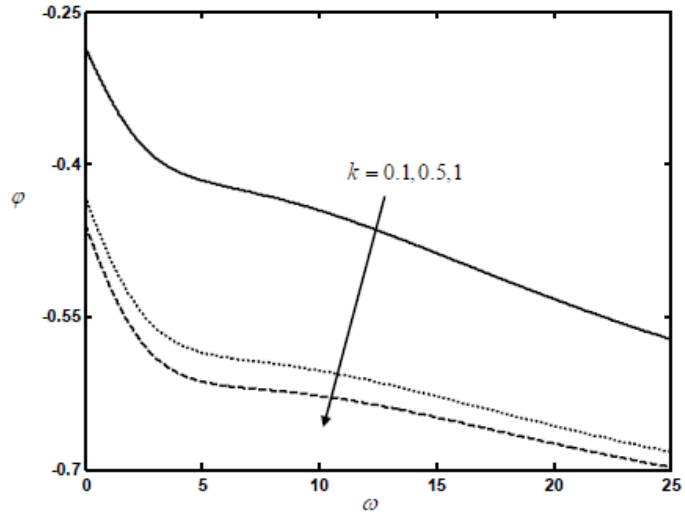

Fig. – 37: Phase angle of the skin-friction for different $k$with $\mathrm{Re} = 1$, $A = 5$, $t = 0$, $N = 1$, $M = 2$, $Pe = 0.7$, $Gr = 1$, $Gm = 1$, $\Omega = 5$, $k1 = 0.5$, $S = 0.1$, $S_0 = 2.5$ and $Sc = 0.22$.

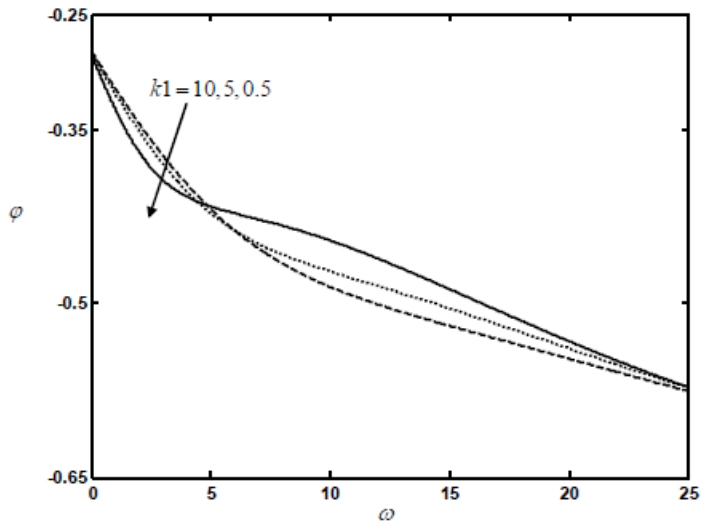

Fig. – 38: Phase angle of the skin-friction for different $k1$with $\mathrm{Re} = 1$, $A = 5$, $t = 0$, $N = 1$, $M = 2$, $Pe = 0.7$, $Gr = 1$, $Gm = 1$, $k = 0.1$, $\Omega = 5$, $S = 0.1$, $S_0 = 2.5$ and $Sc = 0.22$.

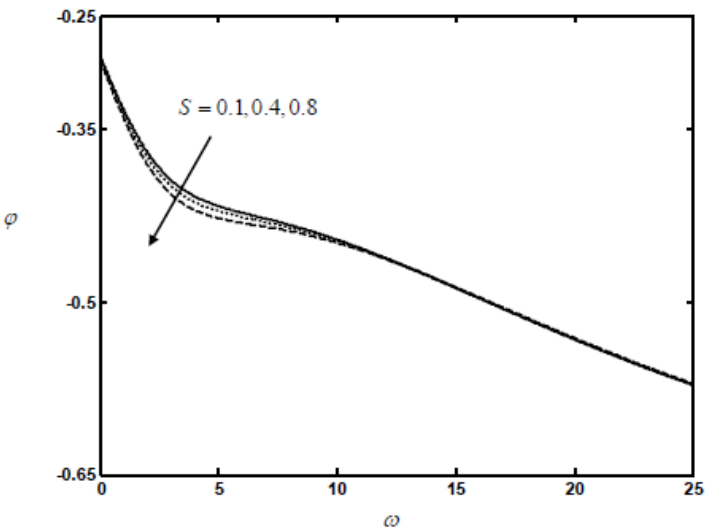

Fig. – 39: Phase angle of the skin-friction for different $S$with $\mathrm{Re} = 1$, $A = 5$, $t = 0$, $N = 1$, $M = 2$, $Pe = 0.7$, $Gr = 1$, $Gm = 1$, $k = 0.1$, $k1 = 0.5$, $\Omega = 5$, $S_0 = 2.5$ and $Sc = 0.22$.

© 2014, IJMA. All Rights Reserved

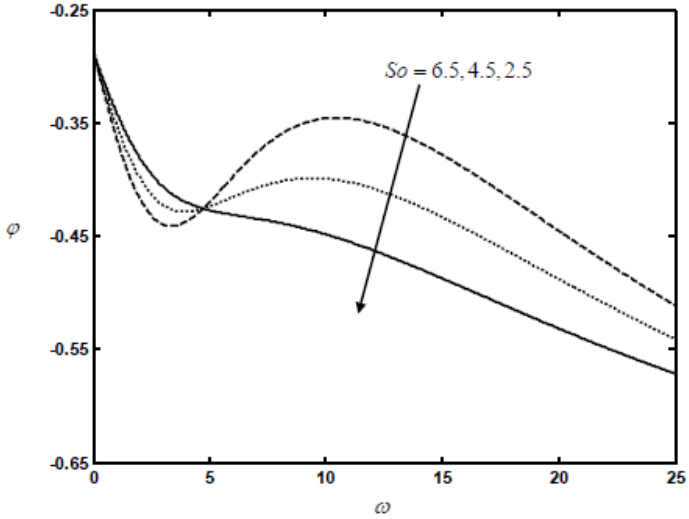

Fig. – 40: Phase angle of the skin-friction for different *So* with $\mathrm{Re}=1$, $A=5$, $t=0$, $N=1$, $M=2$, $Pe=0.7$, $Gr=1, Gm=1$, $k=0.1$, $k1=0.5$, $S=0.1$, $\Omega=5$ and $Sc=0.22$.

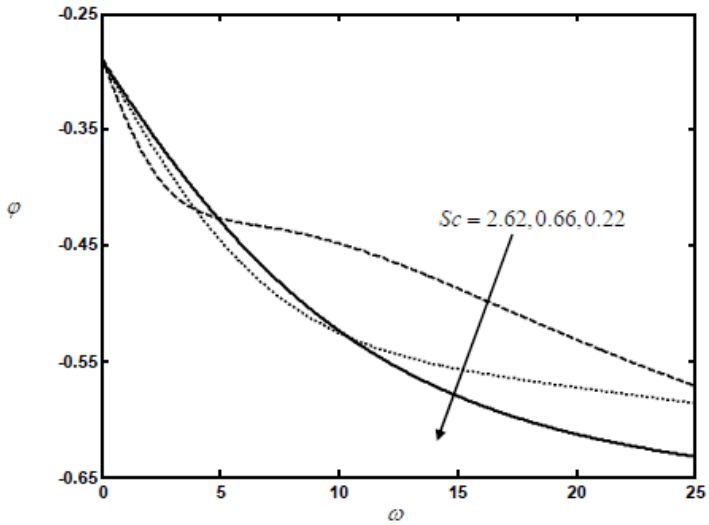

Fig. – 41: Phase angle of the skin-friction for different *Sc* with $\mathrm{Re}=1$, $A=5$, $t=0$, $N=1$, $M=2$, $Pe=0.7$, $Gr=1, Gm=1$, $k=0.1$, $k1=0.5$, $S=0.1$, $\Omega=5$ and $S_0=2.5$.

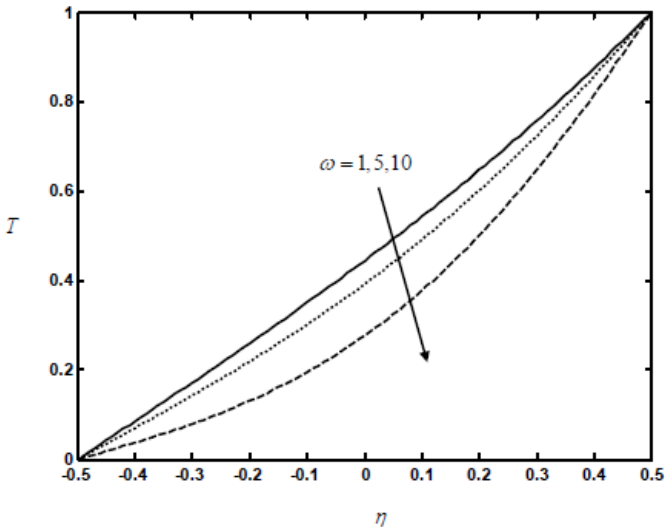

Fig. – 42: The temperature profile for different ω with $t=0, N=1, Pe=0.7, S=0.1$.

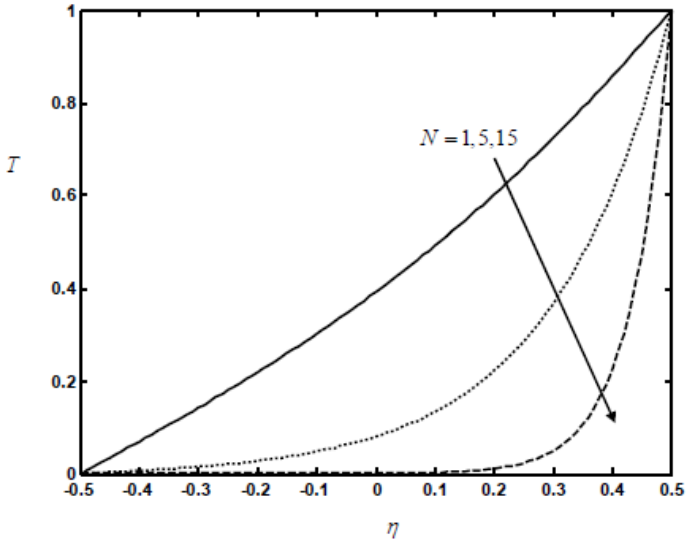

Fig. – 43: The temperature profile for different N with $t = 0,\ \omega = 5, Pe = 0.7, S = 0.1$.

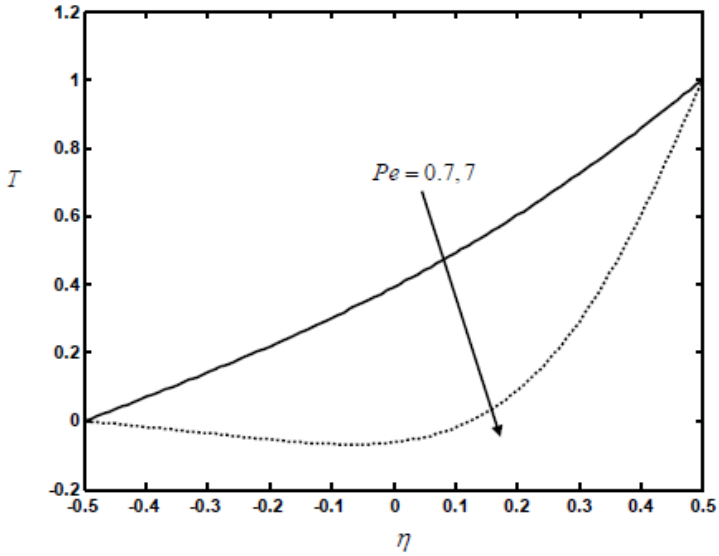

Fig. – 44: The temperature profile for different Pe with $t = 0, N = 1, \omega = 5, S = 0.1$.

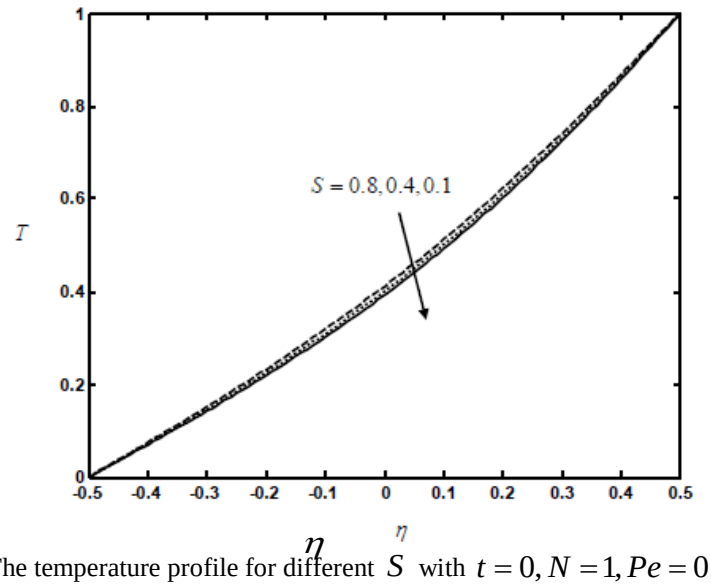

Fig. – 45: The temperature profile for different S with $t = 0, N = 1, Pe = 0.7, \omega = 5$.

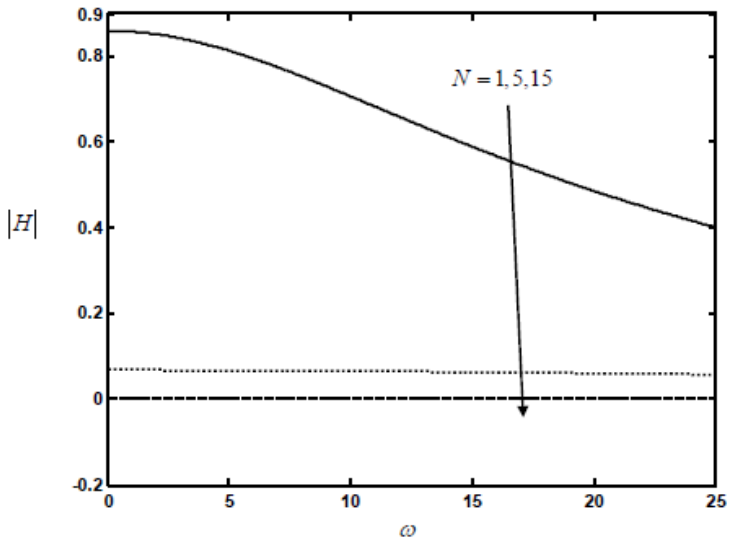

Fig. – 46: Amplitude of the Nusselt number for different N with $t = 0, Pe = 0.7, S = 0.1$.

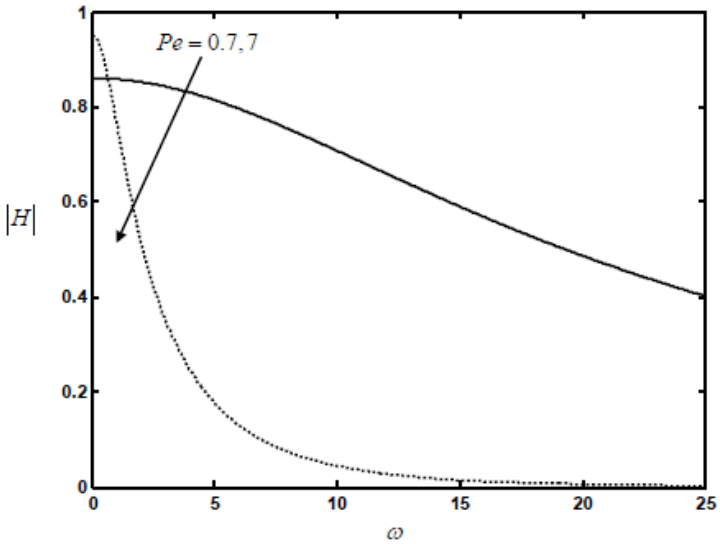

Fig. – 47: Amplitude of the Nusselt number for different Pe with $t = 0, N = 1, S = 0.1$.

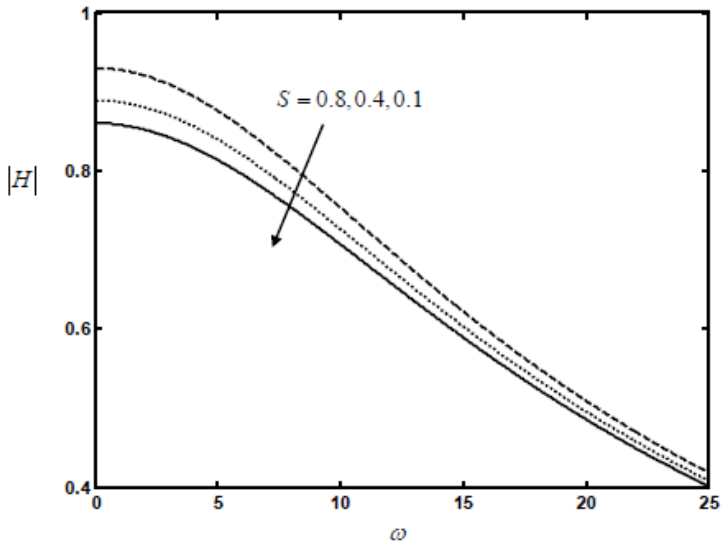

Fig. – 48: Amplitude of the Nusselt number for different S with $t = 0, Pe = 0.7, N = 1$.

© 2014, IJMA. All Rights Reserved

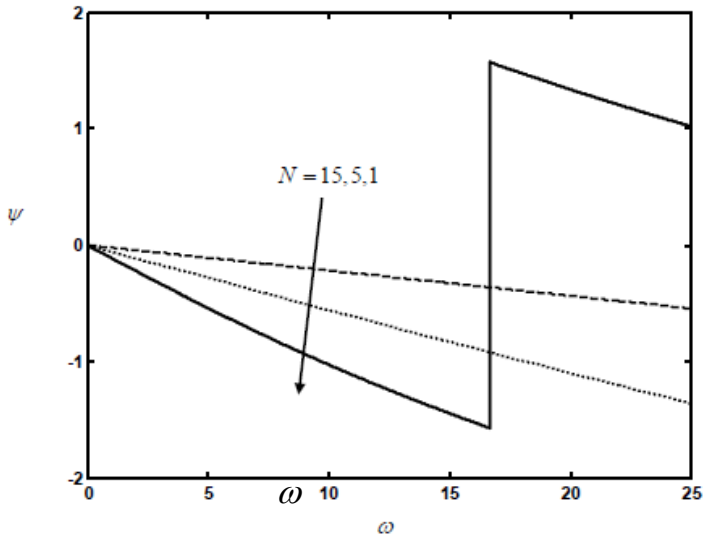

Fig. – 49: The Phase angle of Nusselt number for different N with $t = 0, Pe = 0.7, S = 0.1$.

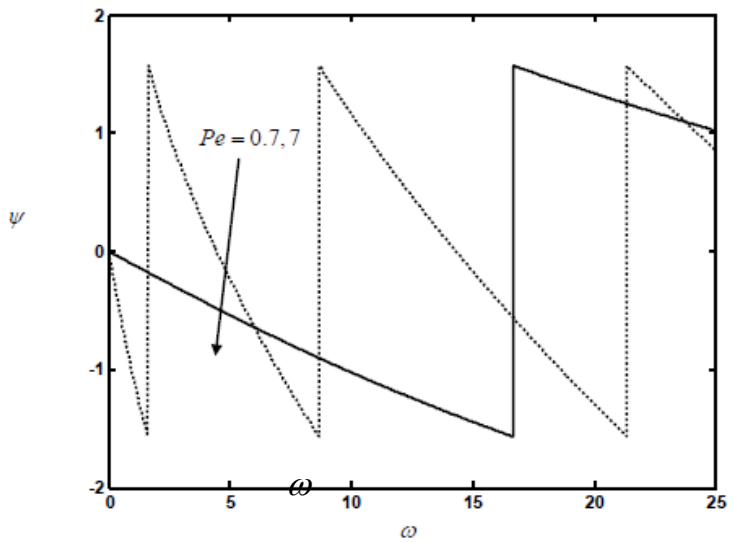

Fig. – 50: The Phase angle of Nusselt number for different Pe with $t = 0, N = 1, S = 0.1$.

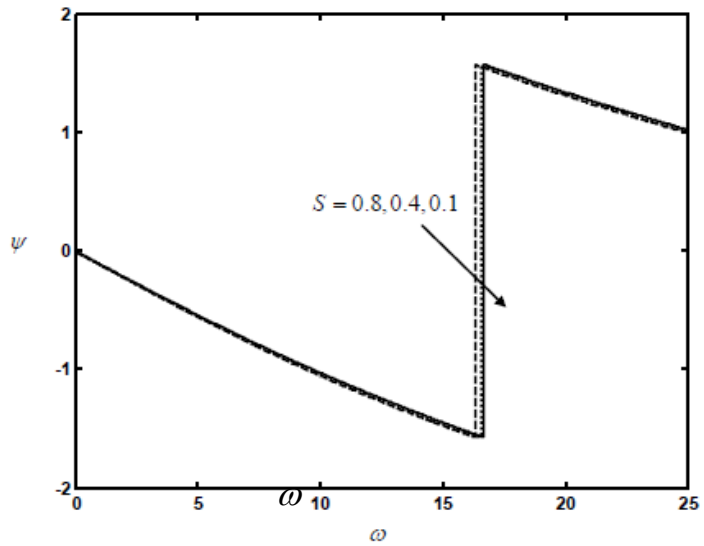

Fig. – 51: the Phase angle of Nusselt number for different S with $t = 0, Pe = 0.7, N = 1$.

© 2014, IJMA. All Rights Reserved

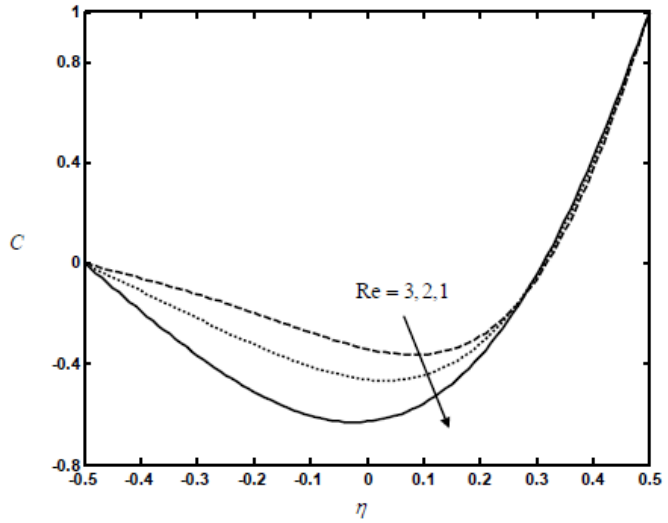

Fig. – 52: The concentration profile for different Re with $t = 0, N = 1, \omega = 5, Pe = 0.7, S = 0.1,$ $Sc = 0.22, So = 2.5$ and $k1 = 0.5.$

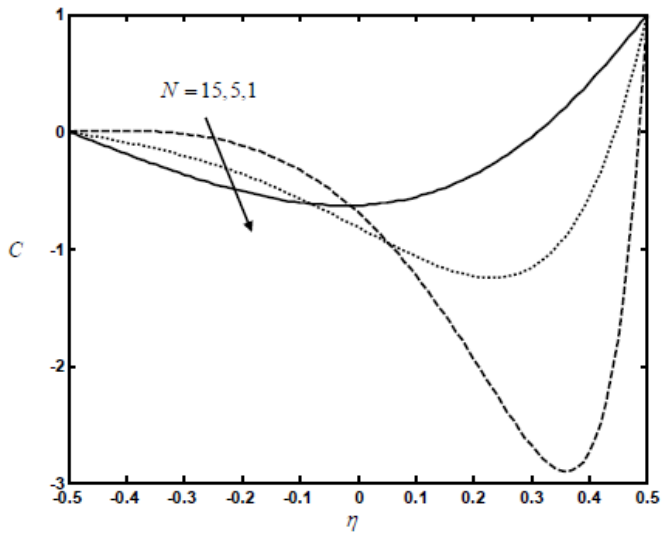

Fig. – 53: The concentration profile for different N with $t = 0, \mathrm{Re} = 1, \omega = 5, Pe = 0.7, S = 0.1,$ $Sc = 0.22, So = 2.5$ and $k_1 = 0.5.$

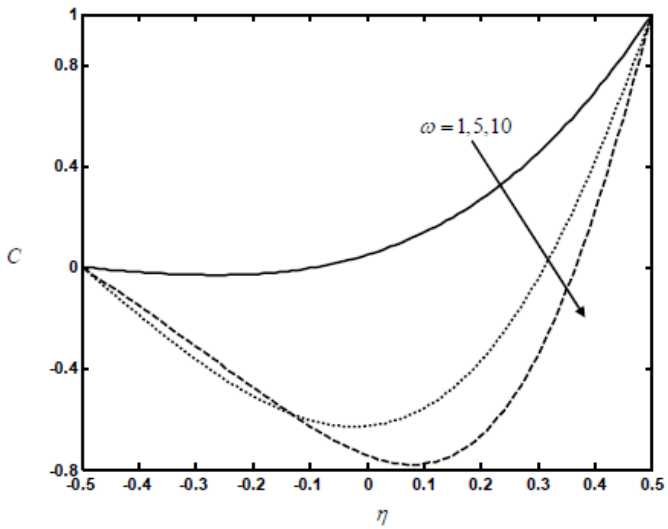

Fig. – 54: The concentration profile for different ω with $t = 0, N = 1, \mathrm{Re} = 1, Pe = 0.7, S = 0.1,$ $Sc = 0.22, So = 2.5, k1 = 0.5.$

© 2014, IJMA. All Rights Reserved

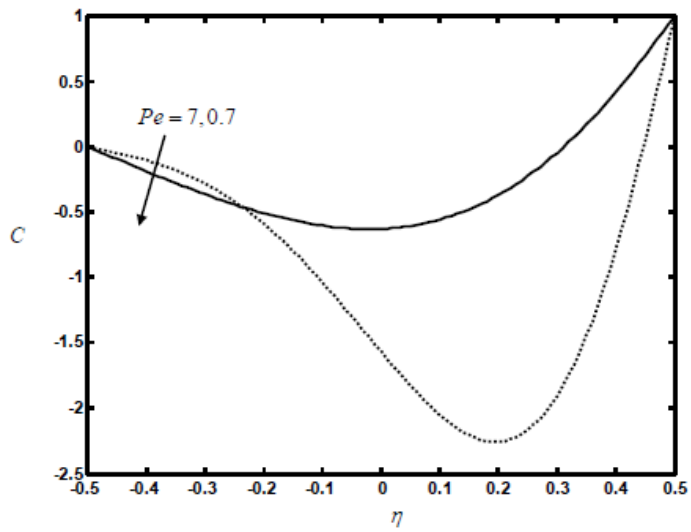

Fig. – 55: The concentration profile for different Pe with $t = 0, N = 1, \omega = 5, Re = 1, S = 0.1$, $Sc = 0.22, So = 2.5, k1 = 0.5.$

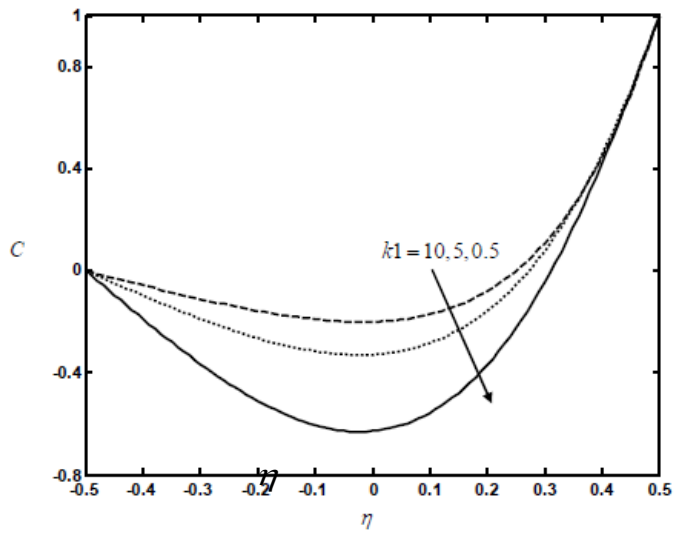

Fig. – 56: The concentration profile for different $k1$ with $t = 0, N = 1, \omega = 5, Pe = 0.7, S = 0.1,$ $Sc = 0.22, So = 2.5, \mathrm{Re} = 1.$

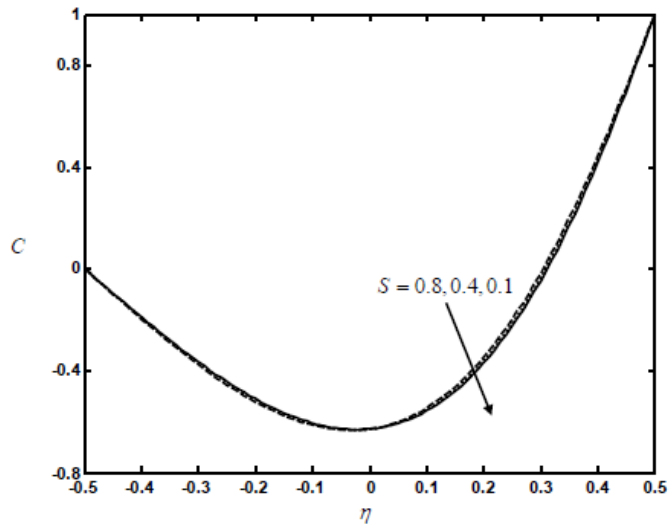

Fig. – 57: The concentration profile for different S with $t = 0, N = 1, \omega = 5, Pe = 0.7, \mathrm{Re} = 1,$ $Sc = 0.22, So = 2.5, k1 = 0.5.$

© 2014, IJMA. All Rights Reserved

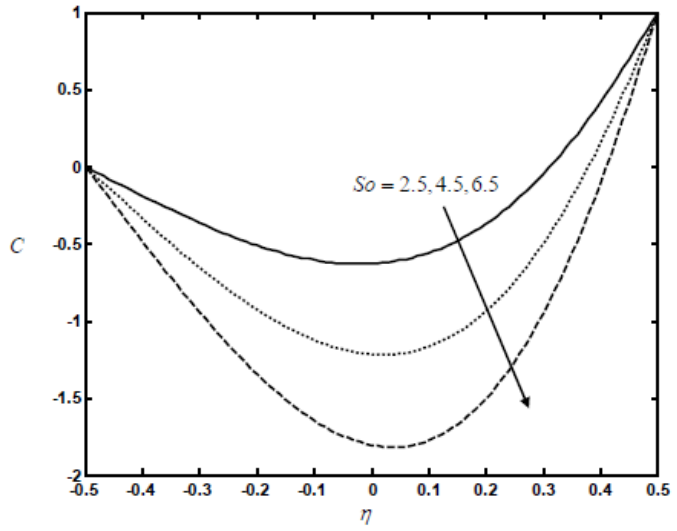

Fig. – 58: The concentration profile for different So with $t = 0, N = 1, \omega = 5, Pe = 0.7, S = 0.1,$ $Sc = 0.22, \mathrm{Re} = 1, k1 = 0.5.$

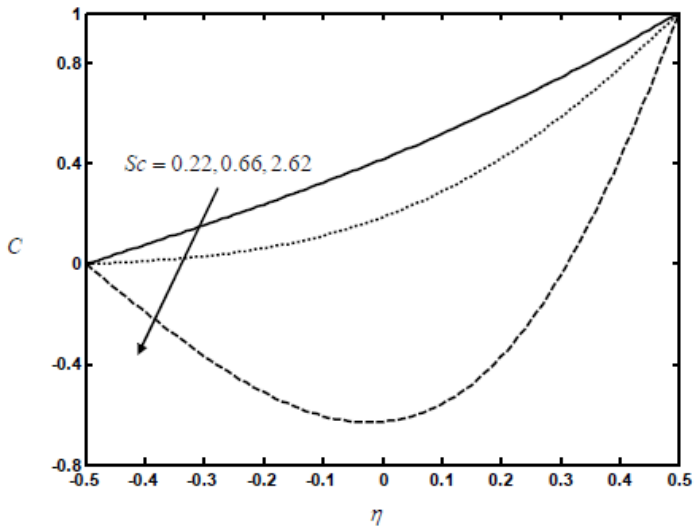

Fig. – 59: The concentration profile for different Sc with $t = 0, N = 1, \omega = 5, Pe = 0.7, S = 0.1,$ $\mathrm{Re} = 1, So = 2.5, k1 = 0.5.$

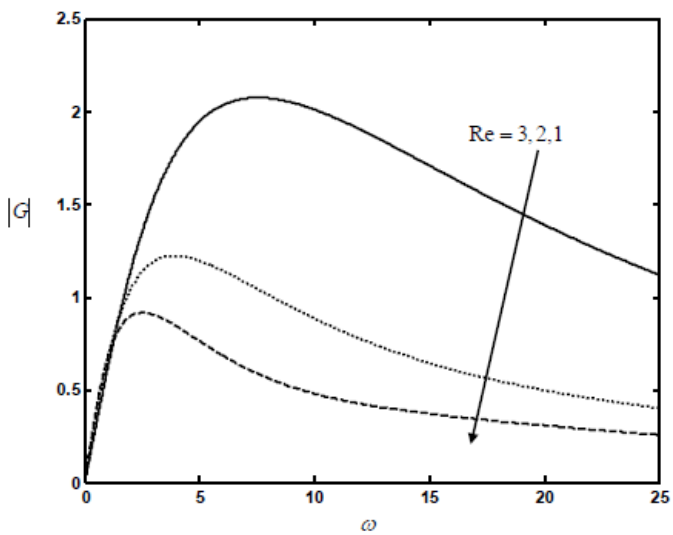

Fig. – 60: Amplitude of the Sherwood number for different Re with $t = 0, N = 1, Pe = 0.7, S = 0.1,$ $Sc = 0.22, So = 2.5, k1 = 0.5.$

© 2014, IJMA. All Rights Reserved

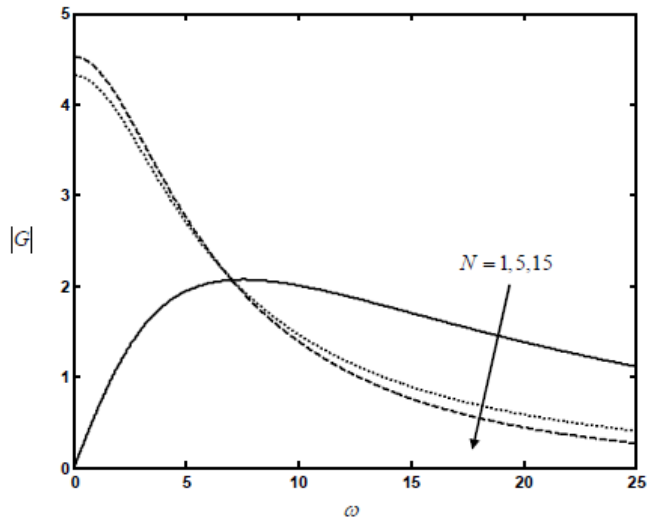

Fig. – 61: Amplitude of the Sherwood number for different N with $t = 0, \mathrm{Re} = 1, Pe = 0.7, S = 0.1,$ $Sc = 0.22, So = 2.5, k1 = 0.5.$

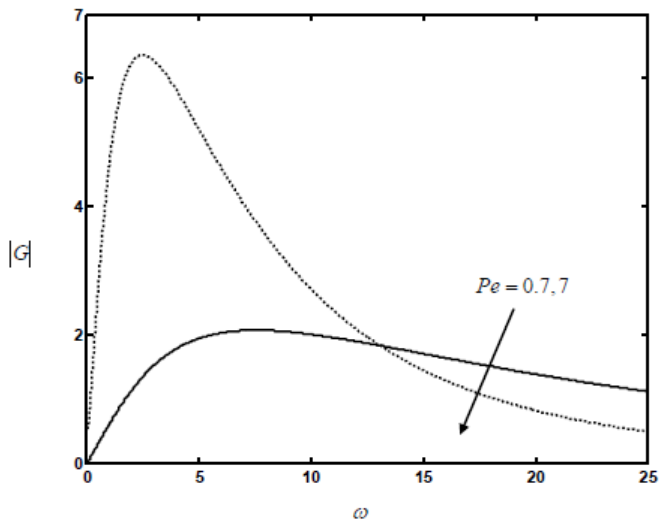

Fig. – 62: Amplitude of the Sherwood number for different Pe with $t = 0, N = 1, \mathrm{Re} = 1, S = 0.1,$ $Sc = 0.22, So = 2.5, k1 = 0.5.$

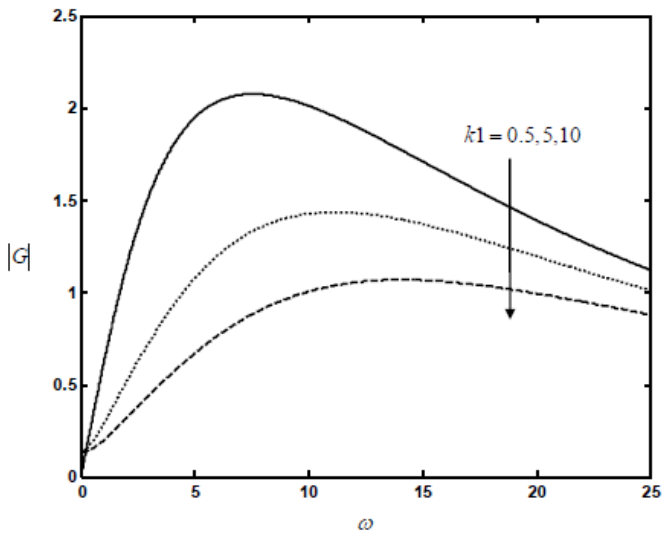

Fig. – 63: Amplitude of the Sherwood number for different $k1$ with $t = 0, N = 1, Pe = 0.7, S = 0.1,$ $Sc = 0.22, So = 2.5, \mathrm{Re} = 1.$

© 2014, IJMA. All Rights Reserved

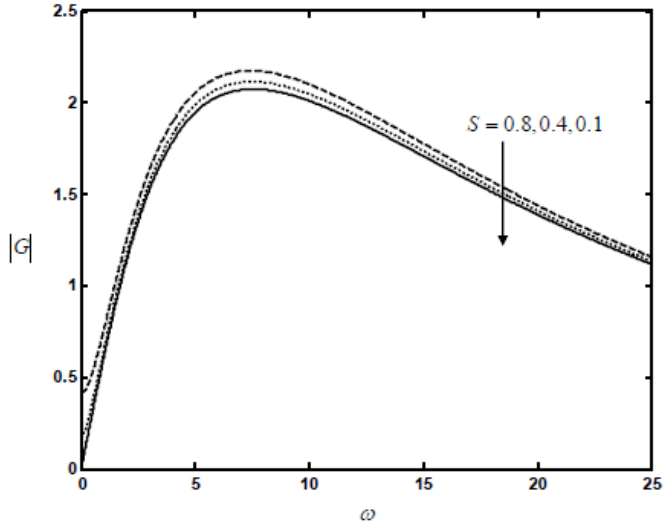

Fig. – 64: Amplitude of the Sherwood number for different S with $t = 0, N = 1, Pe = 0.7, \mathrm{Re} = 1,$ $Sc = 0.22, So = 2.5, k1 = 0.5.$

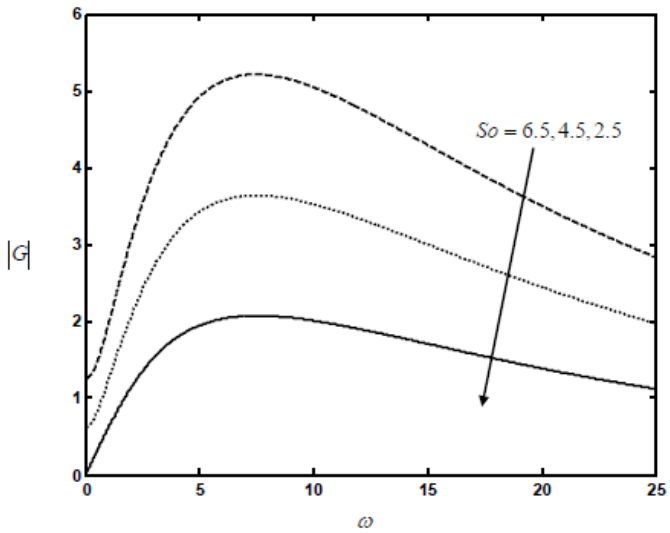

Fig. – 65: Amplitude of the Sherwood number for different So with $t = 0, N = 1, Pe = 0.7, S = 0.1,$ $Sc = 0.22, \mathrm{Re} = 1, k1 = 0.5.$

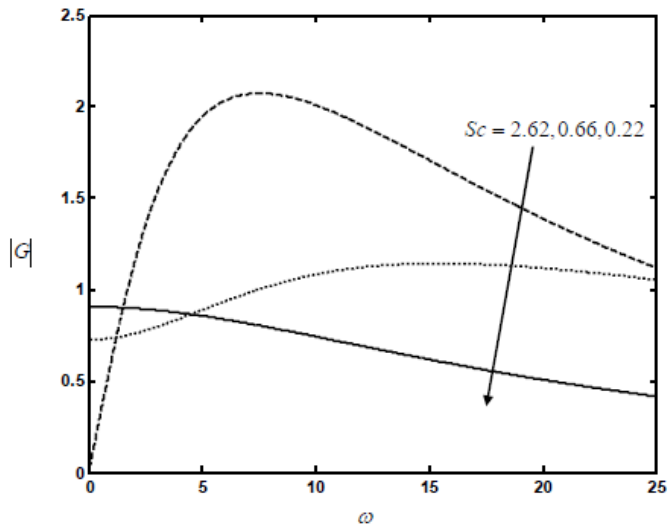

Fig. – 66: Amplitude of the Sherwood number for different Sc with $t = 0, N = 1, Pe = 0.7, S = 0.1,$ $\mathrm{Re} = 1, So = 2.5, k1 = 0.5.$

© 2014, IJMA. All Rights Reserved

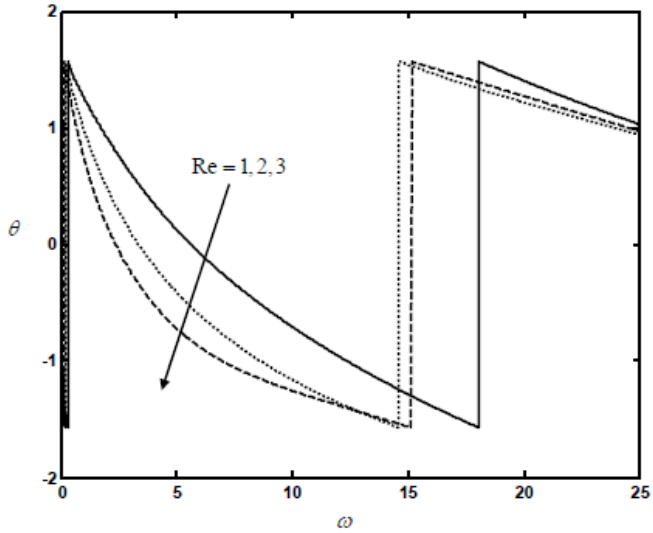

Fig. – 67: Phase angle of the Sherwood number for different Re with $t = 0, N = 1, Pe = 0.7, S = 0.1,$ $Sc = 0.22, So = 2.5, k1 = 0.5.$

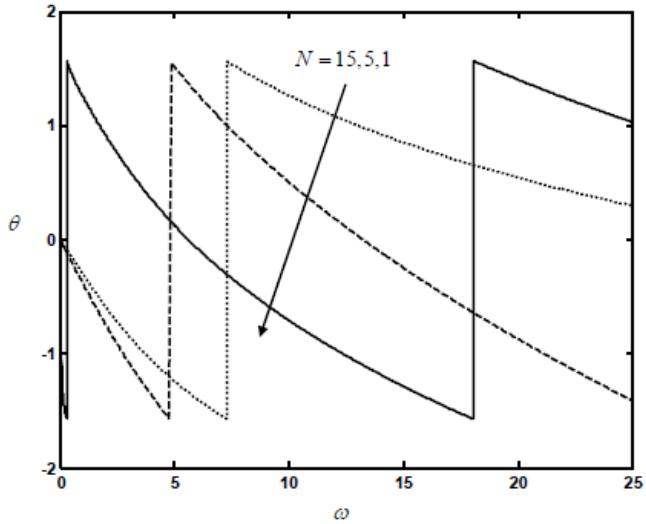

Fig. – 68: Phase angle of the Sherwood number for different N with $t = 0, \mathrm{Re} = 1, Pe = 0.7, S = 0.1,$ $Sc = 0.22, So = 2.5, k1 = 0.5.$

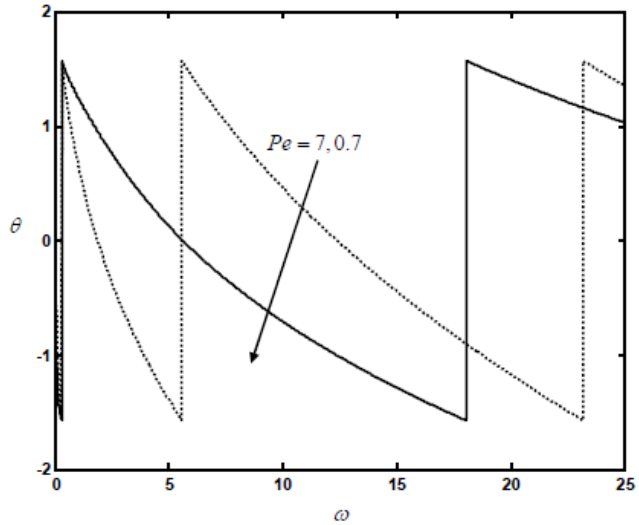

Fig. – 69: Phase angle of the Sherwood number for different Pe with $t = 0, \mathrm{Re} = 1, N = 1, S = 0.1,$ $Sc = 0.22, So = 2.5, k1 = 0.5.$

© 2014, IJMA. All Rights Reserved

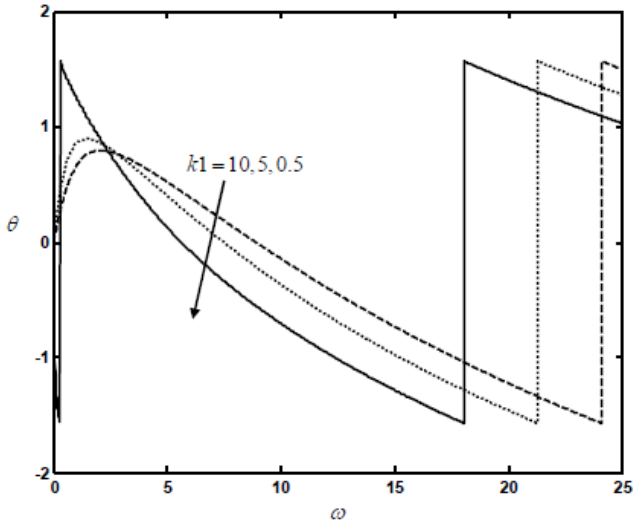

Fig. – 70: Phase angle of the Sherwood number for different $k1$ with $t = 0, \mathrm{Re} = 1, Pe = 0.7, S = 0.1,$ $Sc = 0.22, So = 2.5, N = 1.$

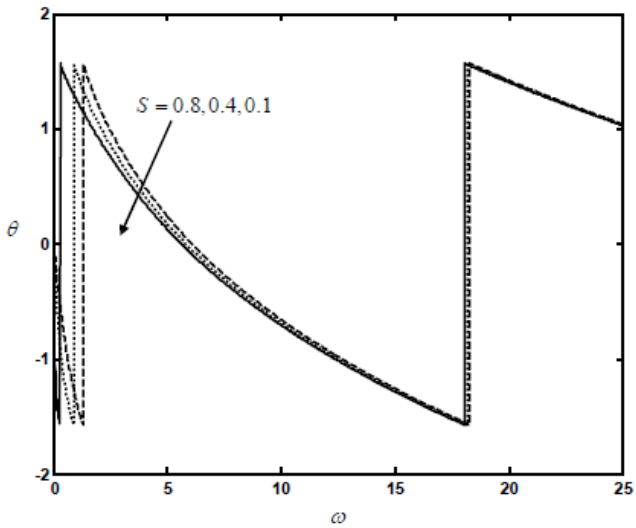

Fig. – 71: Phase angle of the Sherwood number for different S with $t = 0, \mathrm{Re} = 1, Pe = 0.7, N = 1,$ $Sc = 0.22, So = 2.5, k1 = 0.5.$

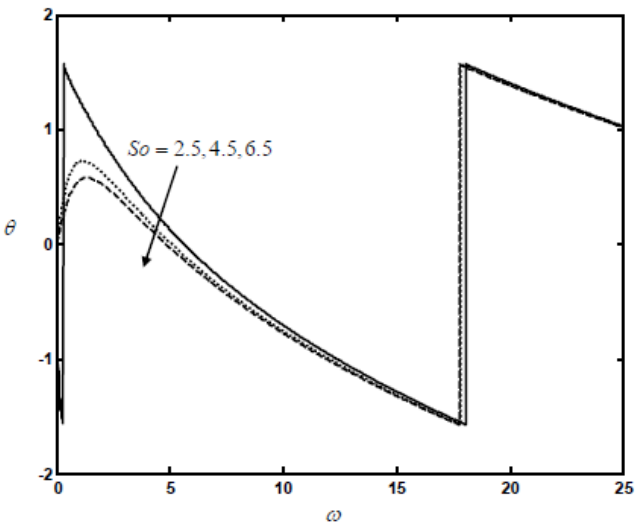

Fig. – 72: Phase angle of the Sherwood number for different So with $t = 0, \mathrm{Re} = 1, Pe = 0.7,\ S = 0.1,$ $Sc = 0.22, N = 1, k1 = 0.5.$

© 2014, IJMA. All Rights Reserved

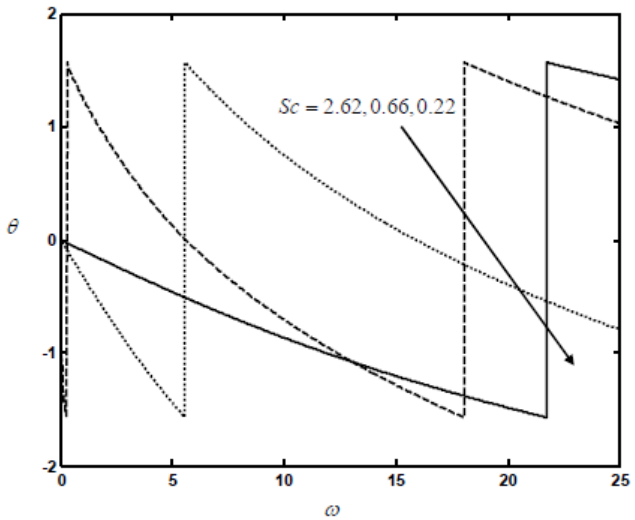

Fig. – 73: Phase angle of the Sherwood number for different Sc with $t = 0, \mathrm{Re} = 1, Pe = 0.7,\ S = 0.1,$ $N = 1, So = 2.5, k1 = 0.5.$

Source of support: Nil, Conflict of interest: None Declared